Investigating the Relative Contribution from Tropical Indo-Pacific SST to Asian Monsoon Precipitation Variability Using LIM

ERIN GUDERIAN,[a] WEIQING HAN,[a] PETER WEBSTER,[b] LEI ZHANG,[c] AND EMANUELE DI LORENZO[d]

[a] *Department of Atmospheric and Oceanic Sciences, University of Colorado Boulder, Boulder, Colorado*
[b] *Department of Earth and Atmospheric Sciences, Georgia Institute of Technology, Atlanta, Georgia*
[c] *South China Sea Institute of Oceanology, Chinese Academy of Sciences, Guangzhou, China*
[d] *Department of Earth, Environmental and Planetary Sciences, Brown University, Providence, Rhode Island*

(Manuscript received 31 October 2023, in final form 8 August 2024, accepted 27 August 2024)

ABSTRACT: A critical issue is determining the factors that control the year-to-year variability in precipitation over southern Asia. In this study, we employ a cyclostationary linear inverse model (CS-LIM) to quantify the relative contribution of tropical Pacific and Indian Ocean sea surface temperature anomalies (SSTAs) to the interannual variability of the Asian monsoon, especially Indian summer monsoon rainfall (ISMR). Through a series of CS-LIM experiments, we isolate the impacts of the direct forcing from Pacific SSTAs, Indian Ocean SSTAs, and their interaction on Asian monsoon rainfall variability. Our results reveal distinct patterns of influence with the direct forcing from the Pacific (Indian) Ocean tending to enhance (reduce) the magnitude of precipitation variability, while the Indo-Pacific interaction acts to strongly damp the variability of Asian monsoon precipitation, especially over India. We further investigate these specific impacts on ISMR by analyzing the relationship between tropical Indo-Pacific SSTAs and the leading three empirical orthogonal functions (EOFs) of ISMR. The results from our CS-LIM experiments indicate that the direct forcing from El Niño–Southern Oscillation (ENSO) enhances the variability of the first and third EOFs, while the Indian Ocean SSTA opposes ENSO's effects, which is consistent with previous studies. Our new results show that the tropical Indo-Pacific interaction strongly damps ISMR variability, which is due to the ENSO-induced Indian Ocean dipole (IOD) opposing the direct impacts from ENSO on ISMR. Additionally, reduced ENSO amplitude and duration associated with the Indo-Pacific interaction may also contribute to the damping effect on ISMR, but this requires further study to understand the relevant mechanisms.

KEYWORDS: Indian Ocean; Monsoons; ENSO; Interannual variability

1. Introduction

Southern Asia receives the majority of its annual precipitation over a concentrated 3–4 month period. This rainy season, referred to as the Asian summer monsoon, occurs each year from June to September and plays an important role in sustaining one of the world's most densely populated regions. Even though the Asian monsoon is considered a fairly regular system, the amount of precipitation can vary from year to year, which can have substantial impacts on the local agriculture and economies in the region (e.g., Webster et al. 1998). Despite extensive efforts by the scientific community, the drivers of interannual variability in precipitation over the Asian monsoon region are not fully understood.

Many existing studies have identified El Niño–Southern Oscillation (ENSO) as one of the leading drivers of interannual precipitation variability over southern Asia (e.g., Webster and Yang 1992; Ju and Slingo 1995; Lau and Nath 2000). The positive (negative) phase of ENSO, known as El Niño (La Niña), is associated with warm (cold) sea surface temperature anomalies (SSTAs) in the tropical central and eastern Pacific Ocean. ENSO events are strongly tied to the seasonal cycle with its developing phase often coinciding with the peak of the Asian summer monsoon (i.e., during boreal summer). Thus, numerous studies have investigated ENSO's impact on the monsoon through atmospheric teleconnections and associated changes in the large-scale circulation (e.g., Lau and Nath 2000; Wang et al. 2003; Annamalai and Liu 2005; Hrudya et al. 2021a). During a developing El Niño event in boreal summer, the center of tropical convection that typically occurs over the western Pacific warm pool shifts eastward resulting in suppressed convection and anomalous subsidence over the Asian monsoon region.

Previous studies have found that ENSO can also impact rainfall over southern Asia during its peak in boreal winter and through its decay phase as well. More specifically, the ENSO-induced anomalous circulation over the western North Pacific (WNP) has been shown to strongly influence precipitation over eastern Asia (e.g., Wang et al. 2003). Although the initial development of the anomalous WNP circulation has been tied to ENSO forcing in the tropical Pacific, studies have found that the Indian Ocean is a key component in extending its influence over southern Asia beyond the decay phase of ENSO (Xie et al. 2009; Wu et al. 2010; Chowdary et al. 2019). This influence is often referred to as the Indo-western Pacific Ocean capacitor effect (e.g., Xie et al. 2016), which is also linked to the leading mode of interannual SSTA variability in

Supplemental information related to this paper is available at the Journals Online website: https://doi.org/10.1175/JCLI-D-23-0657.s1.

Corresponding author: Erin Guderian, erin.guderian@colorado.edu

DOI: 10.1175/JCLI-D-23-0657.1

the Indian Ocean known as the Indian Ocean Basin (IOB) mode. The IOB is associated with a basinwide warming or cooling SSTA pattern that occurs in boreal spring, typically following the peak phase of ENSO (Klein et al. 1999). Thus, in addition to prolonging ENSO's impacts over eastern Asia in boreal winter and spring, the IOB also influences precipitation during the subsequent Asian summer monsoon season (Yang et al. 2007, 2010; Chowdary et al. 2019).

In recent decades, particular attention has been paid to the Indian Ocean dipole (IOD) mode, which is the second mode of tropical Indian Ocean SSTA variability and is characterized by opposing SSTA in the eastern and western parts of the equatorial Indian Ocean (Saji et al. 1999; Webster et al. 1999). Numerous studies have investigated the impacts of IOD events on Asian summer monsoon precipitation during the IOD's peak phase in boreal fall (e.g., Ashok et al. 2001), as well as in the subsequent winter and summer monsoon seasons (Yuan et al. 2008; Yang et al. 2010). It has also been shown that the IOD actively interacts with ENSO (e.g., Izumo et al. 2008, 2010; Zhang et al. 2021a) and influences the relationship between ENSO and the Indian summer monsoon (e.g., Ashok et al. 2004; Ummenhofer et al. 2011; Cherchi and Navarra 2013). Both observation-based and modeling studies have demonstrated that independently occurring positive IOD events act to increase the summer monsoon precipitation over India (e.g., Ashok et al. 2004; Sun et al. 2015; Hrudya et al. 2021a). Thus, the co-occurrence of positive IOD events with developing El Niño events in the tropical Pacific can have counteracting effects on the Indian summer monsoon resulting in slightly reduced or near-normal precipitation (Ummenhofer et al. 2011; Cherchi and Navarra 2013). Additionally, it has been suggested that IOD and ENSO can be integral components of the tropical biennial oscillation (Loschnigg et al. 2003; Meehl et al. 2003).

The influence of tropical Indian Ocean SST on Asian monsoon precipitation is not only tied to the leading modes of variability, such as the IOB and IOD. Some previous studies have found that the regional air–sea interactions in the Arabian Sea, Bay of Bengal, and southern Indian Ocean can play an important role in the interannual variability of the Asian monsoon (Meehl 1997; Terray et al. 2003; Izumo et al. 2008; Mishra et al. 2012; Shukla and Huang 2016). In turn, it has also been shown that air–sea coupling over the tropical Indian Ocean can affect ENSO (e.g., Yu et al. 2002; Yu 2008) and can influence the relationship between ENSO and the Indian monsoon (Ummenhofer et al. 2011; Chowdary et al. 2019). Clark et al. (2000) showed that correlations between the Indian summer monsoon and tropical Indian Ocean SSTA can be strongly influenced by ENSO in some regions although less so in other areas, such as the Arabian Sea. Additionally, Lau and Nath (2000) noted that the ENSO-induced SSTA in the Indian Ocean can produce a local air–sea response that opposes the initial impacts on the Asian monsoon resulting in negative feedback between tropical Indo-Pacific SSTA and the monsoon system.

The complex interactions between the tropical Pacific and Indian Oceans have made it difficult to isolate the impacts on Asian monsoon precipitation variability associated with the independent SST forcing from each basin. Previous observational studies have often applied standard statistical techniques, such as multiple linear regression to remove the interactions between specific climate modes (e.g., Clark et al. 2000; Shukla and Huang 2016; Fan et al. 2021). However, a single climate index, such as the Niño-3.4 index, cannot represent the full spatial and temporal variability of ENSO in tropical Pacific Ocean SSTA. Fully coupled Earth system models (ESMs) have also been shown to be a useful tool for investigating the impacts of tropical SST forcing, such as the Pacific pacemaker experiments which aim to isolate ENSO's impacts on global variability (e.g., Zhang et al. 2018). Other studies have utilized atmospheric general circulation models (AGCMs) to investigate the relative forcing of tropical SSTAs on various phenomena. For example, Wu et al. (2010) performed AGCM sensitivity experiments to determine the role of local SSTA compared to remote forcing from the IOB mode in maintaining the western North Pacific anticyclone associated with decaying El Niño events. Similar model sensitivity experiments have also been applied to investigate the forcing of monsoon precipitation (e.g., Annamalai et al. 2005; Li et al. 2010; Mohino et al. 2011; Fan et al. 2013); however, the results of these studies may depend on the model's ability to represent the observed teleconnections.

Therefore, the application of linear inverse models (LIMs) in recent years, following Newman (2007), has proven to be a useful observation-based method that can isolate specific forcing terms associated with the internal dynamics and coupled interactions of complex systems. For example, Zhang et al. (2021b) utilized the LIM technique to investigate the coupled dynamics between the tropical Pacific and Indian Oceans. In a similar study, Zhao et al. (2021, 2023) applied LIM to quantify the role of tropical–extratropical coupled dynamics to North Pacific climate variability and specifically demonstrated that the LIM technique was able to remove both the simultaneous and subsequent tropical impact on North Pacific variability more effectively than other methods, such as simultaneous or lagged linear regression. Recently, the LIM approach has been modified to include the seasonal cycle, referred to as a cyclostationary LIM (CS-LIM; Shin et al. 2021), which has been applied in previous studies to investigate the growth of ENSO events (e.g., Vimont et al. 2022) and explore the interaction between tropical Pacific, Atlantic, and Indian Ocean SSTA (e.g., Kido et al. 2023).

In this study, we utilize the CS-LIM framework to quantitatively assess the impacts of the direct forcing from tropical Pacific SSTA, the direct forcing from Indian Ocean SSTA, and the Indo-Pacific SSTA interaction on the interannual variability of Asian monsoon precipitation. Specifically, we investigate the spatial patterns of monsoon rainfall variability associated with the Indian and Pacific Ocean SSTA forcing and further address the relative contribution from each basin to Indian summer monsoon rainfall (ISMR) by analyzing the leading patterns of variability. This paper is organized as follows: section 2 describes the observational datasets, the CS-LIM, and the CS-LIM experiments; section 3 reports our results; and section 4 provides a summary and discussion.

2. Data and methods

a. Observational datasets and climate indices

Two monthly SST observational datasets were used: the Hadley Centre Sea Ice and Sea Surface Temperature dataset, version 1.1 (HadISST; 1° × 1°; Rayner 2003), and the NOAA Extended Reconstructed SST, version 5 (2° × 2°; Huang et al. 2017). Both datasets were interpolated onto a common 2° × 2° grid, and their averaged SSTs from 1950 to 2019 are used for our CS-LIM experiments. Monthly observations of precipitation over the Asian monsoon region were obtained from the Global Precipitation Climatology Centre (GPCC) land precipitation dataset (version 2020; 2.5° × 2.5°; Schneider et al. 2020) for the same 70-yr period of 1950–2019. The monthly interannual anomalies were computed by removing the monthly climatology (i.e., seasonal cycle and long-term means) in each dataset from 1950 to 2019. Linear trends were also removed prior to our analysis. Additionally, since this study focuses on interannual variability, a 3-month low-pass filter was applied to the monthly precipitation anomalies to remove the large intraseasonal component of precipitation variability. Note that our SSTA and precipitation anomalies also include decadal-to-interdecadal components, in addition to interannual variability.

The Niño-3.4 index was computed to represent ENSO using the average SSTA in the Niño-3.4 region (170°–120°W, 5°S–5°N) of the tropical Pacific. For the IOD, we use the dipole mode index (DMI; Saji et al. 1999) defined as the difference between the average SSTA in the western (50°–70°E, 10°S–10°N) and eastern (90°–110°E, 10°S–0°) parts of the tropical Indian Ocean. The IOB index was determined using the average SSTA computed over the full Indian Ocean Basin domain (35°–115°E, 25°S–25°N). An alternative definition of the IOB index (i.e., the first EOF of tropical Indian Ocean SSTA) as defined by Yang et al. (2007) was also tested, and we obtained essentially the same results.

b. Cyclostationary linear inverse model

Following Penland and Sardeshmukh (1995), the evolution of a state vector $\mathbf{x}$ can be represented as a simple linear system driven by white noise:

$$\frac{d\mathbf{x}}{dt} = \mathbf{L}\mathbf{x} + \xi, \tag{1}$$

where $\mathbf{L}$ is the linear dynamical operator and ξ represents the unpredictable temporal white noise forcing, which may still contain spatial structure (see Penland and Matrosova 1994). Equation (1) can be used to approximate a nonlinear system, in which the linear dynamical operator ($\mathbf{L}$) captures the deterministic seasonal anomaly evolution and represents the predictable component of the system, while ξ is used to approximate the nonlinearities and coupled processes that occur on time scales shorter than seasonal. Note that we are referring to $\mathbf{L}$ as the linear dynamical operator since it contains the linear dynamics of the system; however, it may also contain any nonlinearities that can be linearly parameterizable upon the state vector ($\mathbf{x}$).

The approximate solution of Eq. (1) for a lead time (τ) is given as

$$\hat{\mathbf{x}}(t+\tau) = \exp(\mathbf{L}\tau)\,\mathbf{x}(t). \tag{2}$$

The linear dynamical operator ($\mathbf{L}$) can then be calculated from Eq. (2) as follows:

$$\mathbf{L} = \frac{1}{\tau_0}\ln[\mathbf{C}(\tau_0)\mathbf{C}(0)^{-1}], \tag{3}$$

where $\mathbf{C}(\tau_0)$ and $\mathbf{C}(0)$ are defined as the lag-covariance matrices of $\mathbf{x}$ at lag τ_0 and lag zero, respectively. The covariance matrices may be computed independently for each season resulting in a CS-LIM (Shin et al. 2021) in which the linear dynamical operator is determined using the following equation:

$$\mathbf{L}_j = \frac{1}{\tau_0}\ln[\mathbf{C}_j(\tau_0)\mathbf{C}_j(0)^{-1}] \quad \text{for } j = 1, 2, \ldots, 12. \tag{4}$$

In the CS-LIM, the linear dynamical operator ($\mathbf{L}$) contains a seasonal component of the anomaly evolution. Following Shin et al. (2021), it should be noted that a 3-month running mean was applied to the covariance and lag-covariance matrices in the CS-LIM prior to the calculation of $\mathbf{L}$ in Eq. (4) in order to reduce the sampling uncertainties associated with the CS-LIM construction. For consistency, a 3-month running mean was also applied to the observed SSTA and precipitation anomalies after the construction of the LIM to compare the seasonal patterns of variability from the CS-LIM to that of observations.

The noise forcing ξ is generated based on the eigen analysis of the noise covariance matrix, $\mathbf{Q}$, which can be determined using the fluctuation–dissipation relation (Penland and Matrosova 1994):

$$\frac{d\mathbf{C}(0)}{dt} = \mathbf{L}\mathbf{C}(0) + \mathbf{C}(0)\mathbf{L}^{\mathrm{T}} + \mathbf{Q}. \tag{5}$$

For the CS-LIM, the time derivative of $\mathbf{C}(0)$ for each season can be approximated using a finite difference method (Shin et al. 2021), resulting in the following equation for the noise covariance matrix:

$$\mathbf{Q}_j = \frac{\mathbf{C}_{j+1}(0) - \mathbf{C}_{j-1}(0)}{2\Delta t} - [\mathbf{L}_j\mathbf{C}_j(0) + \mathbf{C}_j(0)\mathbf{L}_j^{\mathrm{T}}] \quad \text{for } j = 1, 2, \ldots, 12. \tag{6}$$

Note that any negative eigenvalues of $\mathbf{Q}$ were set to zero, and the remaining positive eigenvalues were reduced accordingly in order to retain the same amount of total variance in the noise forcing, as done in previous LIM studies (e.g., Penland and Matrosova 1994; Shin et al. 2021). The percent reduction in noise variance due to the removal of the negative eigenvalues was minimal (i.e., less than 2%) for all seasons.

c. CS-LIM construction and experiments

We now apply the empirical–dynamical LIM system to investigate the impacts of tropical Pacific and Indian Ocean

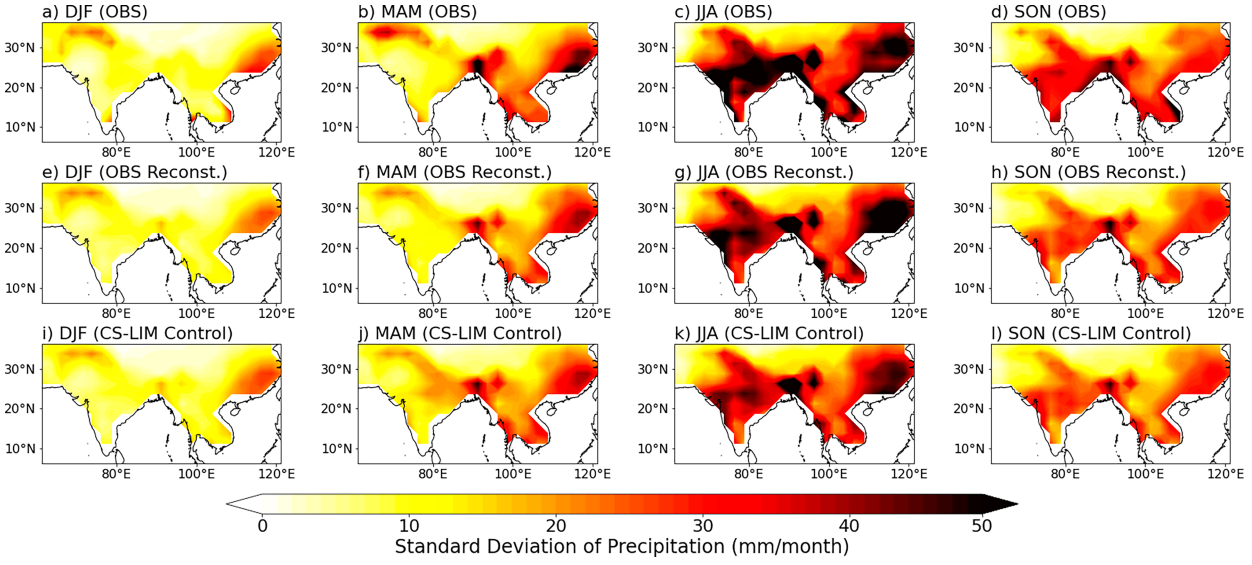

FIG. 1. Standard deviation of precipitation anomalies (mm month^{-1}) over the Asian monsoon region calculated for each season (DJF, MAM, JJA, and SON) for (a)–(d) observations from 1950 to 2019, (e)–(h) reconstructed observations from the 10 leading EOFs and PCs, and (i)–(l) the 70 000-yr CS-LIM control run. Note that for the CS-LIM control run, computing the standard deviation for the full 70 000-yr period is consistent with computing the ensemble mean standard deviation from the 1000 70-yr segments to compare with that of observations.

SSTAs on the interannual variability of Asian monsoon precipitation. Following the approach used in previous LIM studies (e.g., Newman 2007; Zhang et al. 2021b; Kido et al. 2023), we can separate the state vector $\mathbf{x}$ into the different components of a system. For the purposes of our study, the state vector ($\mathbf{x}$) consists of three components: tropical Pacific Ocean SSTA ($\mathbf{x}_P$), tropical Indian Ocean SSTA ($\mathbf{x}_I$), and Asian monsoon precipitation anomalies ($\mathbf{x}_M$). Thus, Eq. (1) can be written as follows:

$$\frac{d}{dt}\begin{bmatrix}\mathbf{x}_M\\ \mathbf{x}_P\\ \mathbf{x}_I\end{bmatrix} = \begin{bmatrix}\mathbf{L}_{MM} & \mathbf{L}_{MP} & \mathbf{L}_{MI}\\ \mathbf{L}_{PM} & \mathbf{L}_{PP} & \mathbf{L}_{PI}\\ \mathbf{L}_{IM} & \mathbf{L}_{IP} & \mathbf{L}_{II}\end{bmatrix}\begin{bmatrix}\mathbf{x}_M\\ \mathbf{x}_P\\ \mathbf{x}_I\end{bmatrix} + \begin{bmatrix}\xi_M\\ \xi_P\\ \xi_I\end{bmatrix}, \tag{7}$$

where $\mathbf{L}$ now contains nine different dynamical operators associated with the internal and coupled interactions within the tropical SST–monsoon system. The elements along the diagonal ($\mathbf{L}_{MM}$, $\mathbf{L}_{PP}$, and $\mathbf{L}_{II}$) represent the internal dynamics for Asian monsoon precipitation, tropical Pacific SSTA, and tropical Indian Ocean SSTA, respectively, since they are computed using the lagged auto-covariance matrices of the state vector. However, they may also inherently contain any impacts from processes other than the three components of the state vector. For instance, the internal monsoon dynamics ($\mathbf{L}_{MM}$) may include the influence on monsoon precipitation anomalies due to changes in Eurasian snow cover (e.g., Vernekar et al. 1995; Sankar-Rao et al. 1996; Liu and Yanai 2002), land surface moisture (e.g., Fu 2003), the Tibetan Plateau (e.g., Li and Yanai 1996; Aiming and Yunqi 1997; Liu and Dong 2013), or aerosols (e.g., Ganguly et al. 2012; Li et al. 2016) since the observed monsoon variability ($\mathbf{x}_M$) contains these impacts. The off-diagonal elements of the linear dynamical operator matrix represent the forcing from one component of the system to another. For example, $\mathbf{L}_{MP}$ represents the forcing from tropical Pacific SSTA onto Asian monsoon precipitation and is computed using the following equation:

$$\mathbf{L}_{MP} = \frac{1}{\tau_0}\ln\left[\langle \mathbf{x}_M(t+\tau_0)\mathbf{x}_P(t)^{\mathrm{T}}\rangle\langle \mathbf{x}_M(t)\mathbf{x}_P(t)^{\mathrm{T}}\rangle^{-1}\right], \tag{8}$$

where the terms in brackets are the covariance matrices between monsoon precipitation anomalies and tropical Pacific SSTA at lag τ_0 and lag zero [i.e., from Eq. (3)]. Thus, the operator $\mathbf{L}_{MP}$ captures the "dynamics" of tropical Pacific SSTA forcing Asian monsoon precipitation anomalies at a lag of τ_0. From Eq. (7), we obtain the following set of LIM equations:

$$\frac{d\mathbf{x}_M}{dt} = \mathbf{L}_{MM}\mathbf{x}_M + \mathbf{L}_{MP}\mathbf{x}_P + \mathbf{L}_{MI}\mathbf{x}_I + \xi_M, \tag{9a}$$

$$\frac{d\mathbf{x}_P}{dt} = \mathbf{L}_{PM}\mathbf{x}_M + \mathbf{L}_{PP}\mathbf{x}_P + \mathbf{L}_{PI}\mathbf{x}_I + \xi_P, \tag{9b}$$

$$\frac{d\mathbf{x}_I}{dt} = \mathbf{L}_{IM}\mathbf{x}_M + \mathbf{L}_{IP}\mathbf{x}_P + \mathbf{L}_{II}\mathbf{x}_I + \xi_I. \tag{9c}$$

In this study, the state vector ($\mathbf{x}$) is composed of the 10 leading principal components (PCs) of tropical Pacific Ocean SSTA ($\mathbf{x}_P$; 130°E–70°W, 25°S–25°N), tropical Indian Ocean SSTA ($\mathbf{x}_I$; 35°–115°E, 25°S–25°N), and precipitation anomalies over the Asia monsoon land region ($\mathbf{x}_M$; 60°–125°E, 5°–35°N; see Fig. 1) accounting for 82.5%, 87.4%, and 47.6% of the variance in each dataset, respectively. Note that the PCs in each component of the state vector have been standardized to have unit variance.

TABLE 1. List of CS-LIM experiments. The individual contributions from Pacific SSTA, Indian Ocean SSTA, and their interaction to precipitation variability over the Asian monsoon region are assessed by computing the differences between the CS-LIM control run and each process experiment (i.e., Control − No P→M, Control − No I→M, and Control − No P↔I, respectively). The same CS-LIM experiments are also performed for the India-only CS-LIM, which differs only by the region of monsoon precipitation over a smaller Indian monsoon area (60°–90°E, 5°–35°N) compared to the broad Asian monsoon region (60°–125°E, 5°–35°N). The tropical Indian and Pacific SSTAs are the same in the two CS-LIMs.

CS-LIM process experiment	Removed forcing term(s) from Eq. (7)	Description
Control	None	Includes all interactions between tropical Pacific Ocean SSTA, tropical Indian Ocean SSTA, and Asian monsoon precipitation.
No P→M	$\mathbf{L}_{MP} = 0$	Direct forcing from Pacific Ocean SSTA onto Asian monsoon precipitation is removed.
No I→M	$\mathbf{L}_{MI} = 0$	Direct forcing from Indian Ocean SSTA onto Asian monsoon precipitation is removed.
No P↔I	$\mathbf{L}_{IP} = \mathbf{L}_{PI} = 0$	Interaction between Pacific Ocean SSTA and Indian Ocean SSTA is removed.

To focus on the precipitation variability over India, an additional CS-LIM was constructed using the 10 leading PCs of precipitation anomalies solely in the Indian monsoon land region (60°–90°E, 5°–35°N) along with the same 10 leading PCs of tropical Pacific and Indian Ocean SSTAs, as described above. Hereafter, this experiment is referred to as the "India-only CS-LIM". By utilizing a smaller spatial domain, the 10 leading PCs of precipitation anomalies used in the India-only CS-LIM account for a larger fraction of the observed variance (60.5%), compared to that used in the broader Asian monsoon CS-LIM (47.6%). We also note that the results are not qualitatively sensitive to the definition of the spatial domains for each region. However, some stability issues can arise for specific CS-LIM experiments when a smaller tropical ocean domain is used (i.e., from 20°S to 20°N).

For both the broad Asian monsoon CS-LIM and India-only CS-LIM, we first obtained a control run, which includes all processes described in Eq. (7) and can be directly compared to observations. Additionally, we performed a series of CS-LIM process experiments to isolate the impacts of tropical Pacific and Indian Ocean SSTAs on Asian monsoon precipitation. These process experiments involve selectively removing specific forcing or coupling terms from Eq. (7) by setting the associated element(s) in the linear dynamical operator matrix to zero (see Table 1). For the purposes of this study, we focus on three key CS-LIM process experiments: 1) elimination of the direct forcing from Pacific SSTA onto the monsoon: denoted as "No P→M," 2) elimination of the direct forcing from the Indian Ocean SSTA onto the monsoon: denoted as "No I→M," and 3) elimination of the interaction between Pacific and Indian Ocean SSTAs: denoted as "No P↔I." The individual contributions from Pacific SSTA, Indian Ocean SSTA, and their interaction with precipitation variability in the Asian monsoon region are assessed by computing the differences between the CS-LIM control run and each CS-LIM process experiment (i.e., Control − No P→M, Control − No I→M, and Control − No P↔I, respectively). The CS-LIM process experiments are performed in the same way for the India-only CS-LIM.

Once we obtained the linear dynamical operator matrix ($\mathbf{L}$) and noise covariance matrix ($\mathbf{Q}$) for each season, we integrated the model forward in time from an initial condition (set to the first-month values of each PC) for 70 000 years with a lag of $\tau_0 = 1$ month and a time step of 1/120 months following the method described in Penland and Matrosova (1994). The 70 000-yr length is 1000 times the 70-yr observational period of 1950–2019, which can be treated as a 1000-member ensemble of a stochastically forced 70-yr LIM simulation. Note that a 1-month lag was selected since the atmospheric response of monsoon precipitation to tropical SSTA forcing is relatively fast (i.e., occurs on time scales shorter than seasonal); however, the linear dynamical operator ($\mathbf{L}$) should be independent of the choice for the initial lag (τ_0) if the dynamics of the state vector ($\mathbf{x}$) are effectively linear (Newman 2007).

For the CS-LIM control run, the forward integration uses the full system equations as shown in Eq. (9) with the appropriate seasonal linear dynamical operator applied for each time step. The CS-LIM process experiments are integrated forward in time in the same way as the control run, but with one (or more) of the linear dynamical operators set to zero (for all seasons) as described in Table 1. For both the control run and process experiments, the resulting CS-LIM time series (that correspond to each PC included in the state vector) are first averaged from the output at the given time step (i.e., 1/120 months) to monthly values in order to compare the results to observations. The monthly PC time series are then projected onto the corresponding observed 10 leading EOFs for each component of the system to obtain CS-LIM predicted datasets with both temporal and spatial variability. Note that the EOFs are computed by projecting the observed standardized PCs back onto the original datasets for each component, which results in EOFs that are in physical units.

The stability of each CS-LIM experiment was assessed following the method described by Shin et al. (2021), noting that the number of PCs selected for each region can affect the stability of the LIM system. In this study, we selected the 10 leading PCs of precipitation anomalies since instabilities occur when more PCs (which are associated with smaller spatial scales and noisier precipitation patterns) are used to compute the linear dynamical operators. Although the 10 PCs only explain 47.6%

(60.5%) of the variance in precipitation anomalies for the Asian (Indian) monsoon domain, the reconstructed seasonal precipitation variability agrees well with observations, except in some localized regions where the variability magnitudes are underestimated (Fig. 1). Therefore, using the 10 leading PCs of monsoon precipitation anomalies serves the purpose of this study. For consistency, we also used 10 leading PCs of SSTA in the tropical Pacific and Indian Ocean regions.

3. Results

We first validate the CS-LIM performance by comparing the results from the CS-LIM control run to observations (section 3a). Then, we analyze the results from the suite of CS-LIM experiments to quantify the impacts of Pacific SSTA, Indian Ocean SSTA, and their interaction on the spatial and seasonal distribution of Asian monsoon precipitation variability (section 3b). We then evaluate the leading three EOFs of ISMR to investigate how the isolated tropical Pacific and Indian Ocean SSTAs individually contribute to the variability of ISMR (section 3c).

a. CS-LIM validation

To evaluate the ability of the CS-LIM in capturing rainfall variability over the Asian monsoon region, we compared the observed standard deviation of precipitation anomalies for each season from 1950 to 2019 to the corresponding results from the 70 000-yr CS-LIM control run (Fig. 1). We note that the mean precipitation anomalies for each 70-yr segment of the CS-LIM are very similar to the mean computed over the full 70 000-yr simulation. Thus, computing the standard deviation for the full 70 000 years is essentially equivalent to computing the ensemble mean standard deviation from the 1000 70-yr segments of the CS-LIM to compare with that of the 70-yr observational record. During boreal winter (DJF), both observations and the CS-LIM control run show enhanced rainfall variability over southeastern China, the southern part of the Indo-Chinese Peninsula, and part of northwestern India (Figs. 1a,e,i), which is consistent with the rainfall variability associated with the East Asian winter monsoon (e.g., Wang et al. 2022). Observations for boreal spring (MAM; Figs. 1b,f) reveal increased variability over southeastern China, over Bangladesh, across the Indo-Chinese Peninsula, as well as over a small region of northwestern India and Pakistan. The CS-LIM control run exhibits similar patterns of increased rainfall variability in MAM to observations although with a slight extension of the signal into central India (Fig. 1j). For boreal summer (JJA) and fall (SON), both observations (Figs. 1c,d,g,h) and the CS-LIM control run (Figs. 1k,i) display the strongest signals of enhanced precipitation variability across most regions of southern Asia, consistent with the increased fluctuations in precipitation during the peak of the Asian summer monsoon (JJA) and its subsequent season of SON, consistent with Ashok et al. (2007) and Hrudya et al. (2021a). The CS-LIM control run successfully simulated the spatial patterns and magnitudes of the precipitation variability, agreeing remarkably well with the observed precipitation variability in all seasons reconstructed from the 10 leading EOFs (Figs. 1e–h).

To validate the linearity of the state vector ($\mathbf{x}$), we performed the LIM "tau test" to check whether the linear dynamical operator ($\mathbf{L}$) is independent of the choice for τ_0 (Penland and Sardeshmukh 1995), by comparing the CS-LIM predicted lag-covariance to that of observations for lags longer than the prescribed training lag (i.e., longer than 1 month). Following the method described by Shin et al. (2021), the results of the CS-LIM tau test for tropical Pacific and Indian Ocean SSTAs were consistent with those from previous LIM studies (e.g., Newman et al. 2011; Shin et al. 2021; Zhang et al. 2021b), while the results for monsoon precipitation anomalies indicated that the linear approximation of this system may only be valid for lags up to about 5–6 months for both the broad Asian monsoon region CS-LIM and India-only CS-LIM (figures not shown). This is expected due to the shorter persistence of monthly precipitation anomalies compared to that of SSTAs. Our choice of $\tau_0 = 1$ month in combination with the model's ability to capture the observed spatial and seasonal variability of precipitation anomalies in the Asian monsoon region (Fig. 1) suggests that the CS-LIM is suitable for this study. Further validation of the India-only CS-LIM is provided in section 3c.

b. Impacts of tropical Indo-Pacific SSTA on precipitation over the Asian monsoon region

To assess the individual contributions from Pacific SSTA, Indian Ocean SSTA, and their interaction with precipitation variability over the Asian monsoon region, we compute the seasonal standard deviation difference between the CS-LIM control run and each process experiment, as described in section 2c and Table 1. The results reveal distinct patterns of influence from tropical Pacific and Indian Ocean SSTAs on rainfall variability over the Asian monsoon region (Fig. 2). For the direct forcing from the Pacific onto the monsoon, our results show enhanced rainfall variability (i.e., increased standard deviation of precipitation anomalies) over eastern China during DJF (Fig. 2a), which can be explained by ENSO's impact on the East Asian winter monsoon (e.g., Zhang et al. 2022). This enhanced variability is also present in the preceding and subsequent seasons of SON and MAM (Figs. 2b,d). The strongest signals of enhanced precipitation variability during MAM are located over the Indo-Chinese Peninsula (Fig. 2b), which is consistent with the results from recent studies showing that ENSO has the strongest influence on precipitation over the Indo-Chinese Peninsula during the ENSO decaying spring through the induced anomalous circulation in the western North Pacific (Yang et al. 2020; Li et al. 2021; Ge et al. 2021). Additionally, we see an increase in the standard deviation over India, especially in the central core monsoon region during JJA (Fig. 2c), indicating that the remote forcing from the tropical Pacific SSTA onto the monsoon acts to enhance the variability of ISMR.

For the direct forcing from the Indian Ocean onto the monsoon (Figs. 2e–h), there is generally reduced rainfall variability over many regions in southern Asia, in particular, for eastern China and the Indo-Chinese Peninsula during MAM (Fig. 2f) and over India during JJA (Fig. 2g). Thus, Pacific and Indian Ocean SSTAs are associated with opposite impacts on Asian

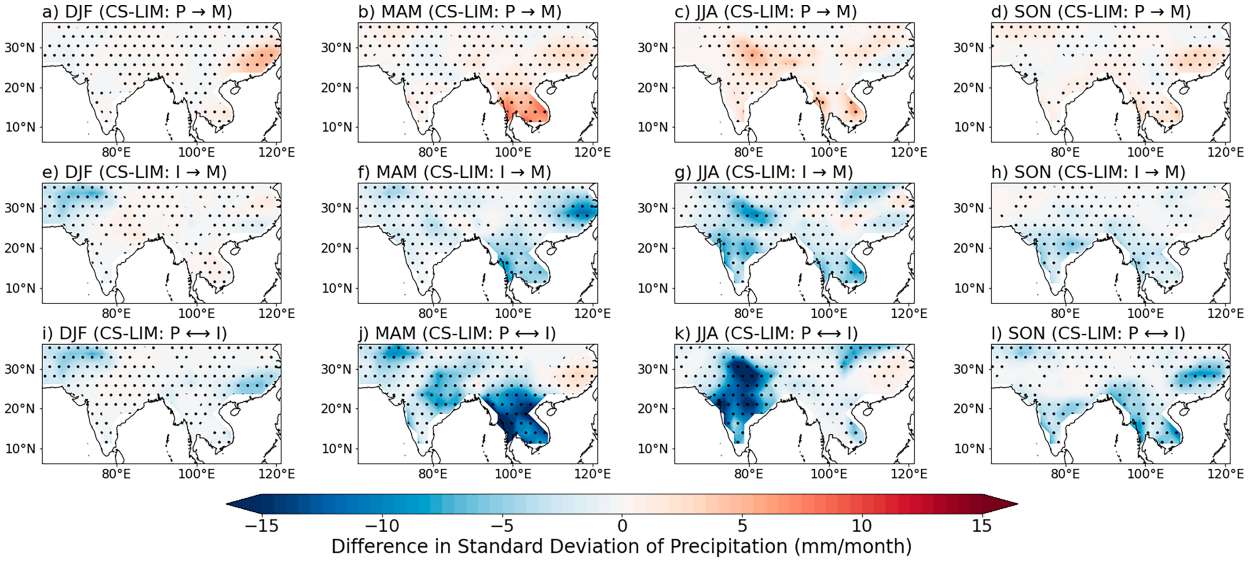

FIG. 2. Difference in the standard deviation of precipitation anomalies (mm month^{-1}) over the Asian monsoon region for each season (DJF, MAM, JJA, and SON) between the CS-LIM control run and the CS-LIM process experiment when (a)–(d) the direct forcing from Pacific Ocean SSTA is removed, (e)–(h) the direct forcing from Indian Ocean SSTA is removed, and (i)–(l) the interaction between Pacific and Indian Ocean SSTAs is removed. Stippling indicates the difference in standard deviation is significant at the 99% confidence level.

monsoon precipitation variability over these regions during boreal spring and summer. This suggests that the forcing from Indian Ocean SSTAs weakens the enhanced precipitation variability induced by ENSO during the Asian summer monsoon and especially for ISMR.

Similarly, for the Indo-Pacific interaction (Figs. 2i–l), there is a stronger reduction in precipitation variability during boreal spring over the Indo-Chinese Peninsula (Fig. 2j) and over India during JJA (Fig. 2k). There is also reduced variability over eastern China during SON (Fig. 2l) and DJF (Fig. 2i). These results imply that Indo-Pacific interaction acts to oppose the impacts from the Pacific during the different stages of ENSO's development but enhances the impacts from Indian Ocean SSTAs particularly during the Asian summer monsoon. We also note there is slightly enhanced rainfall variability over eastern China in MAM and JJA (Figs. 2j,k). Physically, this is consistent with ENSO in the tropical Pacific and the ENSO-induced IOB mode in the Indian Ocean both acting to sustain the anomalous circulation over the western North Pacific and prolong ENSO's influence on precipitation over eastern China (Annamalai et al. 2005; Chowdary et al. 2019).

Overall, these results suggest that while the monsoon–Indian Ocean internal coupled processes, such as the negative feedback of cross-equatorial ocean heat transport to the monsoon, can regulate the Asian monsoon and weaken its variability (Webster et al. 2002), the interaction between tropical Pacific and Indian Ocean SSTAs acts to further dampen the monsoon variability, especially over India. Although previous studies have discussed the negative feedback of ENSO-induced tropical Indian Ocean SSTA forcing, which opposes ENSO's impact on the South Asian monsoon (e.g., Lau and Nath 2000), the magnitude and spatial pattern of reduced precipitation variability specifically due to the Indo-Pacific SSTA interaction has not, to our knowledge, been previously quantified. Since a complete analysis of the relevant physical mechanisms explaining these patterns of enhanced and reduced precipitation variability for each season is beyond the scope of the current study, we instead focus on the India-only CS-LIM results for JJA (i.e., Figs. 2c,g,k) to specifically address the contribution of tropical Indo-Pacific SSTAs to the variability of ISMR.

c. *Impacts of tropical Indo-Pacific SSTA on Indian summer monsoon rainfall*

We now attempt to understand further how the direct forcing from the Pacific, the direct forcing from the Indian Ocean, and the Indo-Pacific interaction each individually impact the variability of ISMR by analyzing the results from the India-only CS-LIM. To do this, we first compute the three leading EOFs of JJA precipitation anomalies over India for the 70-yr observational period from 1950 to 2019 and for each 70-yr segment of the India-only CS-LIM control run. Since the leading three EOFs are the dominant modes of JJA precipitation variability over India which explain the largest percentage of observed and CS-LIM predicted variance, they may provide insight into how the direct forcing from the Pacific, the direct forcing from the Indian Ocean, and the Indo-Pacific interaction act to either enhance or reduce the variability of ISMR, as shown in Figs. 2c, 2g, and 2k. Note that the leading EOFs of ISMR are computed only for the JJA season of precipitation anomalies and are therefore different from the EOFs/PCs that were computed over all months and used to construct the state vector ($\mathbf{x}_M$, as described in section 2c).

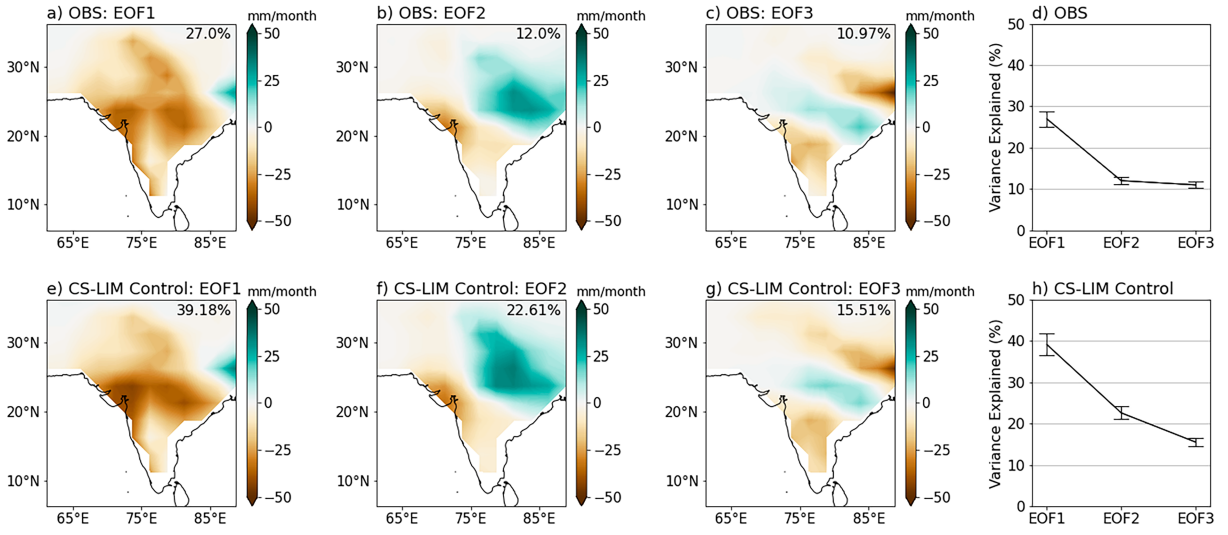

FIG. 3. Leading three EOF spatial patterns of JJA precipitation anomalies (mm month^{-1}) over India (a)–(c) for observations from 1950 to 2019 and (e)–(g) for a single 70-yr segment of the India-only CS-LIM control run. The percentage of explained variance for each mode for (d) observations and (h) the India-only CS-LIM control run with error bars calculated following North et al. (1982). The percentage of explained variance is also shown in the upper-right corner for each EOF.

The spatial patterns of the leading three EOFs of ISMR are shown in Fig. 3. The EOFs have been normalized to be in physical units of precipitation anomalies by projecting the standardized PCs of ISMR onto the JJA precipitation anomalies over India for observations and the India-only CS-LIM control run. The first mode (EOF1) explains 27% of the variance and shows precipitation anomalies with the same sign over the majority of India except for a small region in the northeast (Fig. 3a). The second mode (EOF2) accounts for 12% of the variance and shows a dipole pattern with enhanced precipitation over central and northeastern India accompanied by reduced precipitation over the southwestern part (Fig. 3b). The third mode of ISMR (EOF3) shows a tripole pattern with negative precipitation anomalies over southern and northeastern India accompanied by positive precipitation anomalies over central India (Fig. 3c), accounting for 11% of the variance, which is not well separated from EOF2 statistically (Fig. 3d).

For the India-only CS-LIM control run, we selected a single 70-yr segment (of the 1000-member ensemble) that displayed EOF patterns closely resembling observations (Figs. 3e–g). Note that the ensemble average EOF patterns for the India-only CS-LIM control run are also consistent with observations for each of the three leading modes of ISMR (Fig. S1 in the online supplemental material). The corresponding PC time series for the CS-LIM control EOFs were obtained by projecting the single 70-yr segment EOF spatial patterns of ISMR (shown in Figs. 3e–g) onto the JJA precipitation anomalies for the full length of India-only CS-LIM control run. The spatial correlation coefficients between the leading three EOF patterns for the single 70-yr segment of the India-only CS-LIM control run and those in observations indicate a high degree of consistency: 0.97 for EOF1, 0.96 for EOF2, and 0.95 for EOF3. However, the explained variance associated with the leading modes of ISMR in the 70-yr segment of the India-only CS-LIM control run is larger than that of observations (Figs. 3d,h). This difference is expected since the India-only CS-LIM contains the 10 leading PCs of precipitation anomalies over the Indian monsoon region, accounting for only 60% of the total observed variance. Consequently, the leading modes of ISMR in the control run account for a larger percentage of the variance compared to the observational data despite using the same length of time (i.e., 70 years) to compute the leading EOF modes. Additionally, we note that in observations, there is minimal separation between EOF2 and EOF3 (Fig. 3d); however, in the CS-LIM control run, we see a much clearer separation between EOF2 and EOF3 (Fig. 3h), which implies they can be considered independent modes of variability.

We now attempt to verify that the leading EOFs of ISMR in the India-only CS-LIM control run have the same relationships to tropical Pacific and Indian Ocean SSTAs as in observations. Then, we analyze the results of the India-only CS-LIM process experiments to investigate how the direct forcing from the Pacific, the direct forcing from the Indian Ocean, and the Indo-Pacific interaction each contribute to the variability of the leading three modes of ISMR.

1) COMPARISON BETWEEN CS-LIM CONTROL AND OBSERVATIONS

Before we can analyze the results from the India-only CS-LIM process experiments, it is necessary to confirm that the CS-LIM control run can capture the observed relationships between the leading three EOFs of ISMR and tropical Pacific and Indian Ocean SSTAs. To do this, we regress the JJA tropical Pacific and Indian Ocean SSTAs onto the standardized leading three PCs of ISMR for both observations (Figs. 4a–c

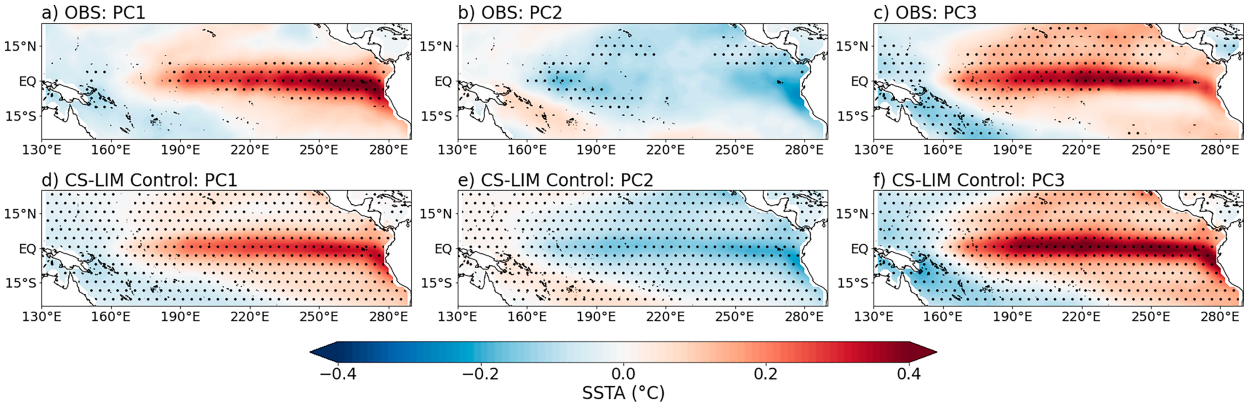

FIG. 4. Regression of JJA tropical Pacific Ocean SSTA (°C) onto the leading three PCs of ISMR for (a)–(c) observations and (d)–(f) the India-only CS-LIM control run. Stippling indicates the regression coefficients are significant at the 90% confidence level for observations and 99% confidence level for the CS-LIM control run.

and 5a–c) and the India-only CS-LIM control run (Figs. 4d–f and 5d–f). Note that for the CS-LIM control run, the leading PCs of ISMR are standardized based on the standard deviation of the single 70-yr segment PCs that correspond to the EOF patterns shown in Figs. 3e–g.

In observations, PC1 is associated with positive SSTAs in the tropical Pacific Ocean with a maximum in the eastern tropical Pacific and extending to the central basin (Fig. 4a), indicating a relationship between ISMR EOF1 and ENSO. Additionally, we see an overall basinwide warming pattern in the tropical Indian Ocean (i.e., resembling the IOB pattern) associated with EOF1 of ISMR (Fig. 5a) although the SSTAs are not statistically significant in most regions of the basin. These results are consistent with previous studies indicating that the first mode of ISMR, associated with reduced (enhanced) rainfall over most regions of the Indian subcontinent, is tied to El Niño (La Niña) events and the closely related positive (negative) IOB mode (e.g., Mishra et al. 2012; Syed and Kucharski 2016; Shukla and Huang 2016). The results for the regression of tropical Pacific and Indian Ocean SSTAs onto PC1 of ISMR in the India-only CS-LIM control run are similar to observations although with statistically significant SSTAs throughout the tropical Pacific and Indian Oceans owing to the long record of the CS-LIM (Figs. 4d and 5d).

For the second mode of ISMR, which is associated with a dipole pattern of rainfall with dry (wet) anomalies in the southwest (northeast) regions of India (Figs. 3b,f), the regression of tropical Pacific SSTA onto PC2 for both observations and the India-only CS-LIM control run shows an overall cooling pattern of SSTAs over most of the basin (Figs. 4b,e), with cold SSTA corresponding to reduced (enhanced) ISMR over southwest (northeast) India. However, the only statistically significant anomalies for the 70-yr observational record are located in the western-central Pacific equatorial region

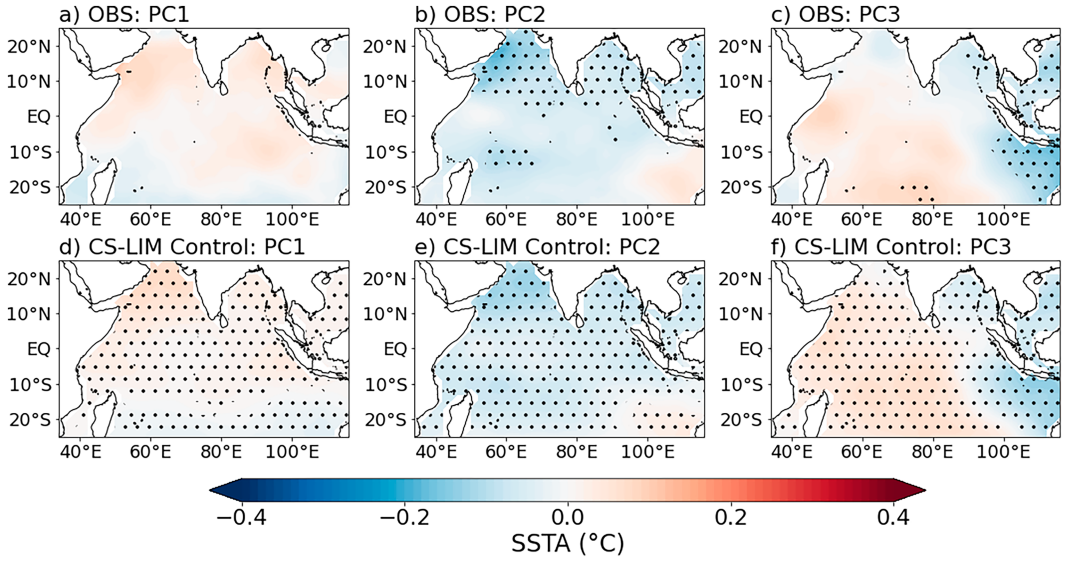

FIG. 5. As in Fig. 4, but for tropical Indian Ocean SSTA.

(160°–190°E), which covers part of the Niño-4 region, off-equatorial regions (190°–220°E), as well as in the northeastern tropical Pacific. This boreal summer SSTA pattern in the tropical Pacific is consistent with the observed SSTA pattern during the decay phase of La Niña events (e.g., Chen et al. 2017; Wu et al. 2021; Gao and Li 2023) and suggests a relationship between PC2 of ISMR and previous year ENSO events, although the regression coefficients are relatively weak (i.e., within ±0.2°C) for both observations and the CS-LIM control run (Figs. 4b,e).

In the tropical Indian Ocean, PC2 of ISMR in observations is associated with significant negative SSTAs in the northern Indian Ocean (both in the Arabian Sea and Bay of Bengal) and southwestern part of the tropical basin off the coast of northeast Madagascar (Fig. 5b). This overall cooling pattern in the tropical Indian Ocean is consistent with the IOB mode, which often occurs following the peak phase of ENSO events (Klein et al. 1999; Yang et al. 2007; Chen et al. 2017). The observed relationship between the dipole pattern of ISMR (i.e., EOF2) and previous ENSO events (including the ENSO-induced IOB mode) is in agreement with previous studies, which have shown that decaying El Niño events and the closely linked positive IOB mode are associated with positive rainfall anomalies over the Western Ghats of the southern Indian Peninsula and negative rainfall anomalies over the monsoon trough region (i.e., negative EOF2 pattern; Yang et al. 2007; Mishra et al. 2012; Chakravorty et al. 2016; Chowdary et al. 2019). The Indian Ocean SSTA regression pattern for PC2 in the India-only CS-LIM control run is similar to that of observations but with statistically significant SSTAs over the entire basin (Fig. 5e).

The regression patterns of tropical Pacific and Indian Ocean SSTAs onto the third mode (PC3) of ISMR, associated with positive precipitation anomalies over central India and negative precipitation anomalies over the southern Indian Peninsula and monsoon trough region (Figs. 3c,g), show significant positive SSTAs across the central and eastern equatorial Pacific which extend northward toward the subtropics in observations (Fig. 4c), indicating a relationship between ISMR PC3 and ENSO. We also note that while the tropical Pacific SSTA regression patterns for PC1 and PC3 are similar in observations (Figs. 4a,c), they exhibit distinct features that have been used to distinguish between the eastern Pacific (EP) and central Pacific (CP) types of El Niño events in some previous studies (e.g., Capotondi et al. 2015; Dandi et al. 2020; Fan et al. 2021). Similar differences can also be seen in the results for the India-only CS-LIM control run (Figs. 4d,f), but the tropical Pacific SSTA regression pattern for PC3 resembles more of a mixed EP- and CP-type El Niño pattern (Fig. 4f). In the tropical Indian Ocean, the observed SSTA regression pattern for PC3 shows statistically significant negative SSTAs in the eastern Indian Ocean and positive SSTAs across most of the rest of the basin with significant anomalies located in the central-west southern Indian Ocean (between about 20° and 25°S) (Fig. 5c). This SSTA pattern is consistent with a developing positive IOD event, which is confirmed by the lagged regression of SON tropical Indian Ocean SSTA (i.e., peak season of IOD) onto PC3 of ISMR (not shown). The India-only CS-LIM control run reproduces the observed SSTA pattern very well, with statistically significant SSTAs over the entire tropical Indian Ocean (Fig. 5f).

To validate further that the India-only CS-LIM is able to capture the observed relationships between the leading three modes of ISMR and ENSO, we analyzed the lead–lag correlation coefficients between each ISMR PC and the seasonal evolution of the Niño-3.4 index (i.e., beginning with previous year ENSO leading the summer monsoon by 1 year and through the peak phase of ENSO in the boreal winter following the JJA of the ISMR PCs), which is shown for observations in Figs. 6a, 6c, and 6e (solid black lines). For comparison, we computed the Niño-3.4 index from the tropical Pacific SSTA in the India-only CS-LIM control run and then determined the ensemble mean correlation coefficients based on the correlations between each 70-yr segment of the ISMR PCs and the corresponding 70-yr segment of the Niño-3.4 index (solid black lines in Figs. 6b,d,f). Similarly, we also computed the correlations between each PC of ISMR and the seasonal evolutions of the IOB and IOD indices in both observations and the India-only CS-LIM control run (dashed and dot–dashed black lines, respectively, in Fig. 6).

Consistent with the observed tropical Pacific SSTA regression pattern (Fig. 4a), PC1 of ISMR, which is associated with reduced rainfall over most of the Indian summer monsoon region, shows a significant positive correlation with ENSO beginning in the late boreal spring of ENSO's developing year (i.e., year 0) and through the following fall and winter seasons with a maximum correlation of $r \approx 0.4$ during the late boreal summer (solid line in Fig. 6a). This observed relationship between developing El Niño (La Niña) events and reduced (enhanced) ISMR is consistent with previous studies (e.g., Mishra et al. 2012; Syed and Kucharski 2016; Shukla and Huang 2016) and is captured by the India-only CS-LIM control run, which shows a significant positive correlation between PC1 and ENSO (maximum $r = 0.3$) during similar seasons as observations (solid line in Fig. 6b).

For the second EOF of ISMR, associated with a dipole pattern of precipitation anomalies, there is a statistically significant negative correlation between PC2 and ENSO in observations (solid line in Fig. 6c; maximum $r = -0.35$), which peaks in the boreal spring (MAM) but decreases below the significance threshold prior to the Indian summer monsoon season (JJA). The India-only CS-LIM control run shows similar seasonally varying ensemble mean correlations between PC2 and ENSO (solid line in Fig. 6d), but they are below the 95% significance level. By contrast, the IOB index shows relatively weak ($r \approx 0.3$), but still statistically significant, negative correlations with PC2 from the previous boreal winter through the peak of the summer monsoon. This is also captured by the CS-LIM control run with the ensemble mean IOB–PC2 correlation exceeding the 95% significance level during JJA (dashed lines in Figs. 6c,d). Since IOB events typically develop following the peak phase of ENSO, these results are consistent with our regression analysis and previous studies showing the impact of decaying ENSO events on ISMR through inducing the IOB mode (Yang et al. 2007; Mishra et al. 2012; Chowdary et al. 2019).

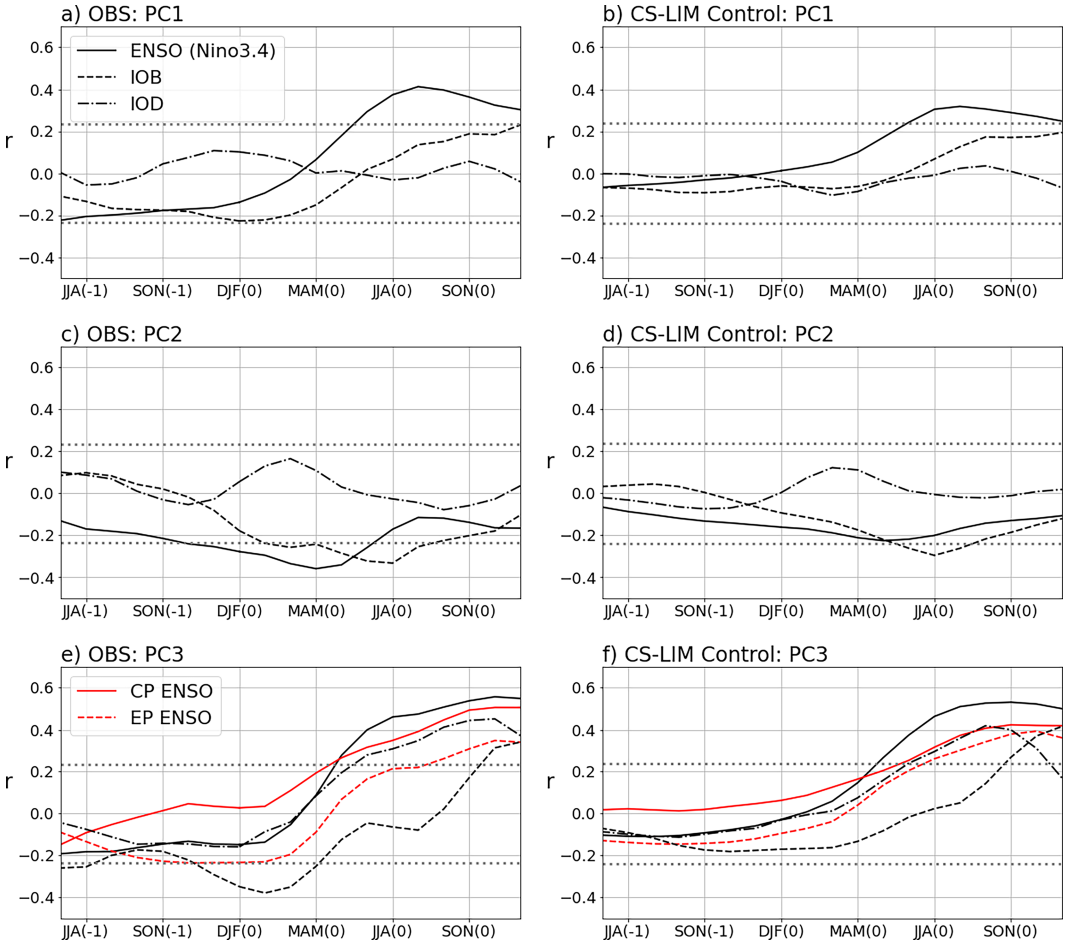

FIG. 6. Correlation coefficients between (top) PC1, (middle) PC2, and (bottom) PC3 of ISMR and each season of the ENSO (solid black lines), IOB (dashed black lines), and IOD (dot–dashed black lines) indices for (a),(c),(e) observations and (b),(d),(f) the India-only CS-LIM control run. Correlations between PC3 and the CP and EP ENSO indices (solid and dashed red lines, respectively) are also shown for (e) observations and (f) the CS-LIM control run. "Year (0)" indicates the correlation was computed using the seasonal ENSO/IOB/IOD index for the same year as the ISMR PCs, while "year (−1)" indicates the correlation with the previous year ENSO/IOB/IOD index. The dotted gray lines indicate the threshold for significance at the 95% confidence level for the observed and CS-LIM ensemble mean correlation coefficients.

The lead–lag correlations for PC3 show that the tripole pattern of ISMR is significantly correlated with both developing ENSO and IOD events (followed by a lagged correlation with IOB after SON) in observations (Fig. 6e) and for the India-only CS-LIM control run (Fig. 6f). Existing studies have shown that positive IOD events are associated with positive precipitation anomalies over India, especially over central India (e.g., Hrudya et al. 2021a), and a similar precipitation pattern as EOF3 can be linked to the impacts of co-occurring ENSO and IOD events (Ashok et al. 2004; Ummenhofer et al. 2013). For observations, there is a significant negative correlation between PC3 and the previous year (DJF) IOB mode (dashed black line in Fig. 6e), but the relationship is not statistically significant in the CS-LIM control run (Fig. 6f). Additionally, by using the CP and EP ENSO indices to replace the Niño-3.4 index (solid and dashed red lines, respectively, in Figs. 6e,f), we find that CP ENSO has a stronger impact on the tripole pattern of ISMR variability than EP ENSO in both observations and the CS-LIM control run although the difference is more subtle for the CS-LIM.

2) ANALYSIS OF CS-LIM PROCESS EXPERIMENTS

The regression and correlation analysis in the previous section demonstrate that the India-only CS-LIM control run is able to capture the observed relationships between the leading three EOFs of ISMR and tropical Pacific and Indian Ocean SSTAs. We now evaluate the relative contribution of tropical Indo-Pacific SSTAs to these leading modes of ISMR by analyzing the results of the India-only CS-LIM process experiments to understand how each isolated forcing acts to enhance or reduce the magnitude of ISMR variability (i.e., the

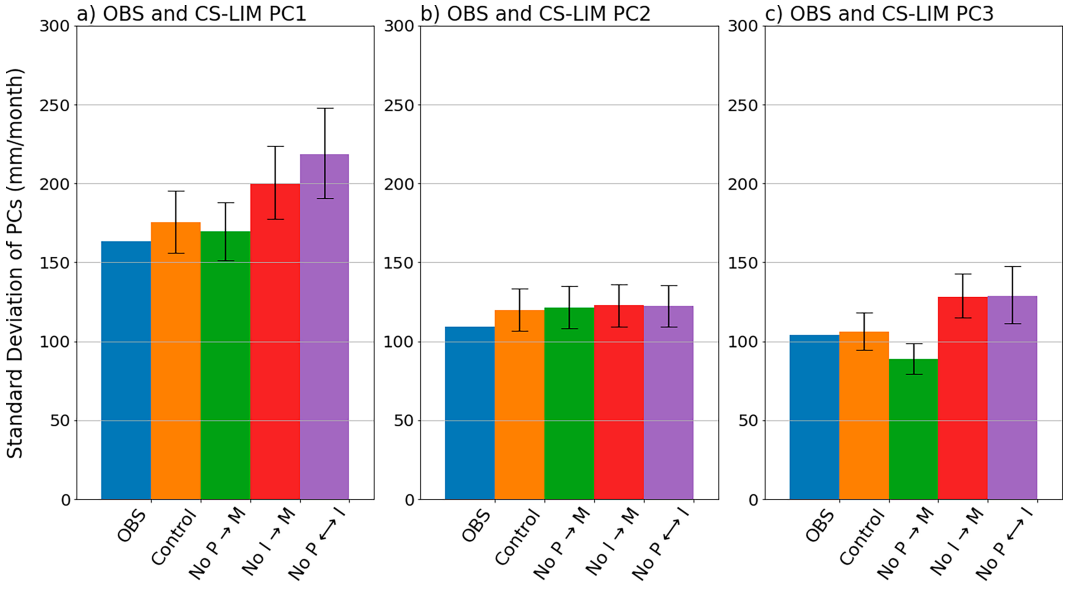

FIG. 7. Standard deviation of ISMR (a) PC1, (b) PC2, and (c) PC3 computed from the JJA monthly precipitation anomalies (mm month^{-1}) over India for observations (blue), the India-only CS-LIM control run (orange), and the India-only CS-LIM process experiments when the direct forcing from Pacific SSTA onto the monsoon is removed (green), when the direct forcing from Indian Ocean SSTA onto the monsoon is removed (red), and when the Indo-Pacific SSTA interaction is removed (purple). For the CS-LIM control run and process experiments, the height of the colored bar indicates the ensemble mean standard deviation, and the error bars denote the 10th and 90th percentiles.

results shown in Figs. 2c,g,k). For each of the India-only CS-LIM process experiments, we obtain a PC time series for the leading three modes of ISMR by projecting the CS-LIM control run EOF patterns (as shown in Figs. 3e–g) onto the JJA precipitation anomalies over India. We then compute the standard deviation of the projected PCs for each 70-yr segment of the India-only CS-LIM process experiments and determine the ensemble mean standard deviation to quantitatively assess how removing the direct forcing from Pacific SSTA, the direct forcing from Indian Ocean SSTA, and the interaction between them each impact the variability of the leading three EOF patterns of ISMR (Fig. 7). For comparison, we also include the standard deviation of each PC of ISMR in observations and the India-only CS-LIM control run and confirm that for all three leading modes, the observed standard deviation is within the range of uncertainty for that of the CS-LIM control run (blue and orange bars in Fig. 7).

For PC1 of ISMR, which is related to developing ENSO events, when we remove the direct forcing from Pacific SSTA onto the monsoon, the ensemble mean standard deviation decreases relative to that of the control run but only slightly (i.e., less than 5%; green bar in Fig. 7a). This decrease agrees with the enhanced ISMR variability by the Pacific SSTA found using the CS-LIM with the larger Asian monsoon domain (Fig. 2c), and the rather weak decrease partly reflects our previous results indicating that the direct forcing from the Indian Ocean and Indo-Pacific interaction are damping ENSO's impact on the monsoon. For example, consider a developing El Niño event in the tropical Pacific which acts to reduce ISMR; if the Indian Ocean and Indo-Pacific interaction are damping this effect, then they would act to enhance ISMR (i.e., induce a negative EOF1 pattern). Since the standard deviation measures the overall variability magnitude (i.e., always positive), then without the direct forcing from tropical Pacific SSTA, the Indian Ocean SSTA and Indo-Pacific interaction can still contribute to the PC1 variation of the ISMR EOF1 pattern and thus to the standard deviation of PC1 in the No P→M experiment. This damping effect of Indian Ocean SSTA and the Indo-Pacific interaction is further supported by the significant increase in the ensemble mean standard deviation of PC1 in the No I→M and No P↔I experiments (red and purple bars in Fig. 7a showing a 14% and 24% increase in the standard deviation, respectively).

The results for the second mode of ISMR show that for all three process experiments, the ensemble mean standard deviation of PC2 remains almost unchanged (green, red, and purple bars in Fig. 7b) relative to that of the control run (orange bar). This indicates that the variability magnitude of the EOF2 dipole pattern of ISMR is not controlled by tropical Indo-Pacific SSTAs at interannual time scales and suggests that other factors, such as internal monsoon variability (section 2c) or processes that occur on time scales shorter than seasonal [i.e., noise in Eq. (7)], mainly influence the variability of ISMR PC2. Therefore, the second mode of ISMR is not further discussed in this study. However, we note that these results are consistent with Mishra et al. (2012), which showed that the intraseasonal fluctuations related to the monsoon active and break periods can also contribute to the interannual variability of the ISMR EOF2 pattern. Other studies have also found a connection between tropical Atlantic SSTAs and a similar northeast–southwest

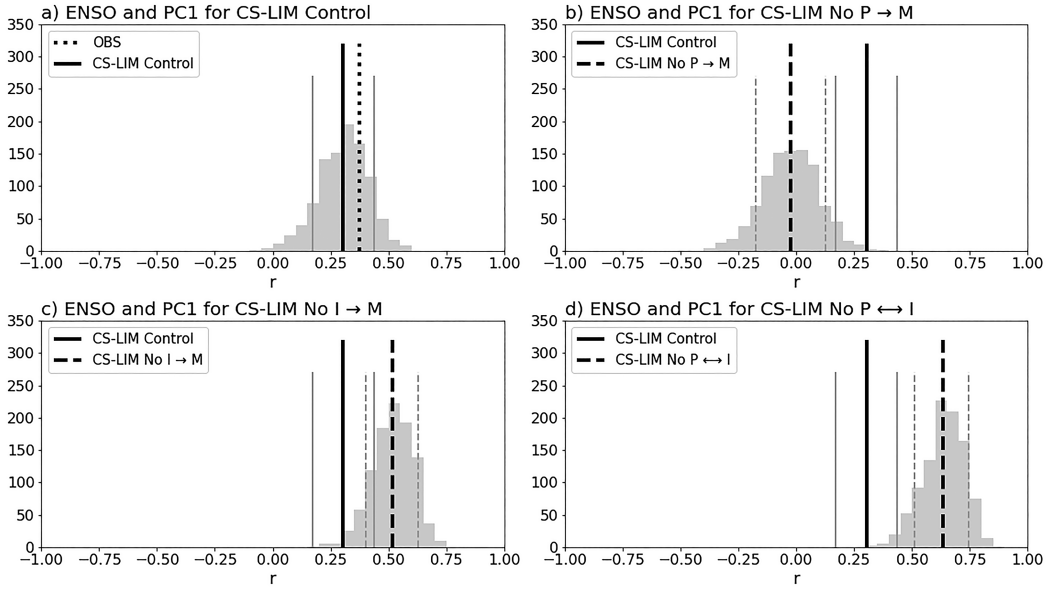

FIG. 8. (a) Simultaneous correlation between the JJA Niño-3.4 index and PC1 of ISMR for observations (black dotted line) and distribution of correlation coefficients between the JJA Niño-3.4 index and PC1 computed for each 70-yr segment of the India-only CS-LIM control run (gray bars). (b)–(d) As in (a), but for the India-only CS-LIM process experiment (b) when the direct forcing from the Pacific onto the monsoon is removed, (c) when the direct forcing from the Indian Ocean onto the monsoon is removed, and (d) when the interaction between the Pacific and Indian Ocean SSTAs is removed. The black solid and dashed lines indicate the ensemble average correlation coefficient for the control run and for each process experiment, respectively. The gray solid and dashed lines indicate the 90% confidence intervals based on each distribution of correlation coefficients.

dipole precipitation pattern over India (e.g., Rong et al. 2010; Syed and Kucharski 2016). Although our current study does not include SSTA in the tropical Atlantic, our results suggest that it may be an important consideration for future studies on ISMR variability.

For the third mode of ISMR, the differences in the standard deviation of PC3 for each of the India-only CS-LIM experiments (relative to the control run) are similar to those of PC1. When we remove the direct forcing from the Pacific onto the monsoon, the PC3 ensemble mean standard deviation decreases by about 17% (green bar in Fig. 7c). When we remove either the direct forcing from the Indian Ocean or the Indo-Pacific interaction, the ensemble mean standard deviation of PC3 increases by about 20% for both experiments (red and purple bars in Fig. 7c). These results suggest that the direct forcing from tropical Pacific SSTA (Indian Ocean SSTA or the Indo-Pacific interaction) can enhance (reduce) the variability of ISMR (as shown in Figs. 2c,g,k) specifically through impacting the first and third leading EOF modes.

To understand how tropical Pacific and Indian Ocean SSTAs influence the variability of ISMR PC1 (associated with developing ENSO events) and PC3 (associated with developing ENSO and IOD events), we first examine the impacts of ENSO on ISMR by computing the correlation coefficients between each 70-yr segment of ISMR PC1 and the corresponding 70-yr segment of the simultaneous boreal summer (i.e., JJA) Niño-3.4 index in each of the India-only CS-LIM experiments. For comparison, we also calculated the ENSO–PC1 correlation for observations and for each 70-yr segment of the India-only CS-LIM control run (Fig. 8a). As expected, when we remove the direct forcing from the Pacific, the ensemble mean correlation between ISMR PC1 and ENSO decreases from $r = 0.3$ in the control run (black solid line in Figs. 8a,b) to near zero ($r = -0.02$) in the No P→M experiment (black dashed line in Fig. 8b). We note that this is also the case for the correlation between ENSO and PC3 of ISMR (Fig. S2). These results demonstrate that the enhanced ISMR variability associated with the direct forcing from the Pacific (i.e., Fig. 2c) can be largely attributed to ENSO's direct impacts on the first and third leading EOFs of ISMR.

However, the relatively weak decrease in the standard deviation of PC1 and PC3 in the No P→M experiment (i.e., Figs. 7a,c) suggests that ENSO is not the only contributing factor to these patterns of monsoon rainfall variability. Thus, in the absence of direct forcing from Pacific SSTA onto the monsoon, tropical Indian Ocean SSTAs (both independent and induced by ENSO) as well as internal monsoon variability and noise [see section 2c, Eq. (7)] can also contribute to the variability of the ISMR EOF1 and EOF3 patterns. When we remove the direct forcing from the Indian Ocean or the Indo-Pacific interaction, the ENSO–PC1 correlations increase to $r = 0.52$ (70% increase) in the No I→M experiment and $r = 0.63$ (108% increase) in the No P↔I experiment (Figs. 8c,d). Thus, the effect of these forcings opposes ENSO's direct impacts on ISMR. Similar results are obtained for the ENSO–PC3 correlations (Fig. S2).

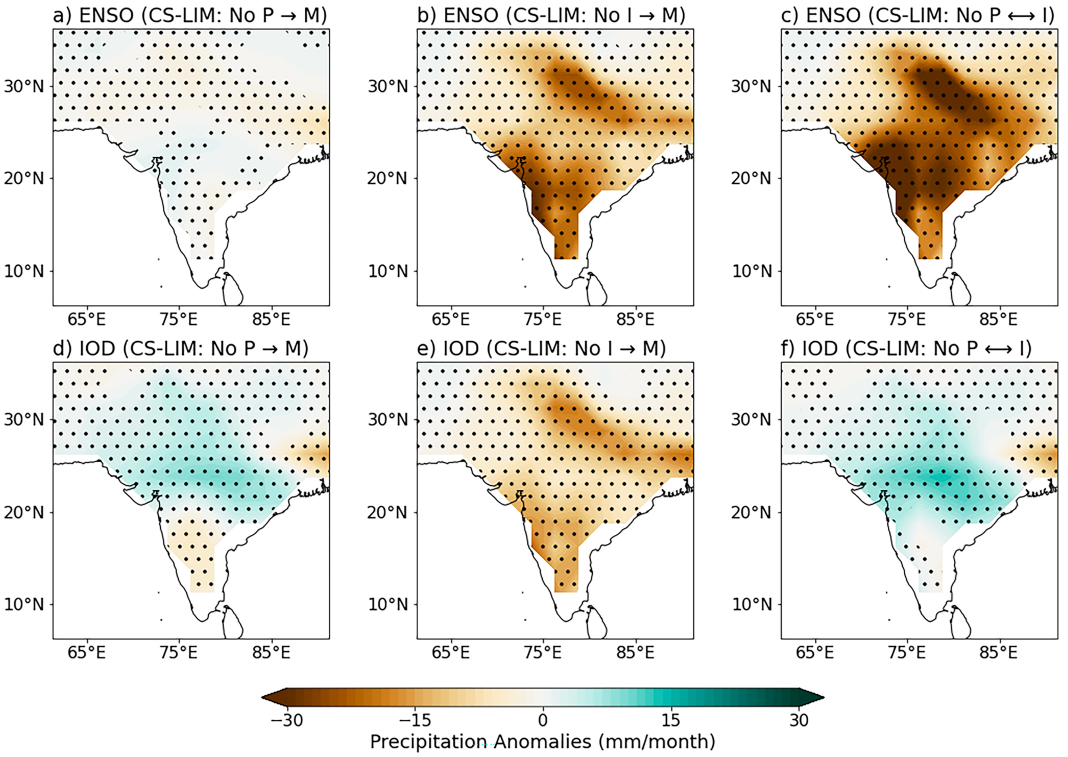

FIG. 9. Regression of JJA monthly precipitation anomalies (mm month^{-1}) over India onto the following peak (top) ENSO (NDJ) and (bottom) IOD (SON) indices for the India-only CS-LIM process experiment (a),(d) when the direct forcing from Pacific SSTA onto monsoon precipitation is removed; (b),(e) the direct forcing from Indian Ocean SSTA onto monsoon precipitation is removed; and (c),(f) the interaction between Pacific and Indian Ocean SSTAs is removed. Stippling indicates the regression coefficients are significant at the 99% confidence level.

The results presented above are further supported by our analyses for the regression of the peak ENSO and IOD indices (i.e., NDJ and SON, respectively) onto the preceding ISMR anomalies for each of the India-only CS-LIM experiments (Fig. 9). When we remove the direct forcing from the Pacific, ENSO has very weak impacts on ISMR (Fig. 9a), while IOD is still associated with a similar ISMR tripole pattern as EOF3 (Fig. 9b). This agrees with the relatively small decrease in the standard deviations of PC1 and PC3 in the No P→M experiment and emphasizes ENSO's contribution to the variability of these EOF patterns. When we remove the direct forcing from the Indian Ocean or the Indo-Pacific coupling, ENSO has a stronger relationship with ISMR (i.e., larger regression coefficients) and the spatial patterns show a combination of EOF1 and EOF3 patterns (Figs. 9b,c), with El Niño (La Niña) further reducing (enhancing) ISMR relative to that in observations and the CS-LIM control run (see Fig. S3). On the other hand, the IOD regression pattern of ISMR resembles that of ENSO when we remove the direct forcing from the Indian Ocean onto the monsoon (Fig. 9e). This is because in the No I→M experiment, ENSO can still trigger co-occurring IOD events, whereas the direct forcing from the Indian Ocean SSTA that opposes ENSO's impacts is removed; therefore, the IOD effect essentially represents ENSO's effect and can explain the increased standard deviation of PC1 and PC3 in this experiment (Figs. 7a,c). These results agree with the coupled model study of Chowdary et al. (2015), showing that the tropical Indian Ocean air–sea coupling acts to oppose El Niño's impacts on ISMR both with and without a co-occurring positive IOD event. When we remove the Indo-Pacific SSTA interaction, IOD events, which are independent of ENSO in the No P↔I experiment (see Fig. S4), generate an ISMR pattern similar to that for No P→M (Fig. 9d), but with ISMR anomalies being weak or slightly positive over southern India (Fig. 9f).

Overall, these results suggest that IOD events act to enhance the variability magnitude of ISMR PC1 and PC3 when they occur independently of ENSO but damp ISMR variability when they co-occur. Previous studies have discussed the relevant physical processes for an El Niño–induced positive IOD event to oppose the impacts of the developing El Niño on ISMR (e.g., Ashok et al. 2004; Ummenhofer et al. 2013). Physically, it is generally understood that El Niño events impact ISMR through the zonal shift in the Walker circulation, which results in anomalous subsidence over the Indian monsoon region and decreases ISMR. Meanwhile, the El Niño–induced anomalous convection can trigger the development of a positive IOD event in boreal summer (e.g., Fischer et al. 2005; Schott et al. 2009) by causing an anomalous wind pattern resembling a strengthened boreal summer monsoon circulation over the tropical Indian Ocean (e.g., Saji et al. 1999; Sun et al. 2015). As such, a developing positive IOD event is associated with southwesterly wind anomalies over the northwest equatorial Indian Ocean, which provide

enhanced moisture transport over India and act to increase ISMR (e.g., Ashok et al. 2001, 2004; Ummenhofer et al. 2011, 2013). Therefore, a positive IOD that co-occurs with an El Niño event damps the El Niño impact, contributing to the reduced ISMR variability due to the direct forcing from Indian Ocean SSTA and the Indo-Pacific interaction (Figs. 2c,g). On the other hand, in the absence of El Niño, independent positive IOD events can develop through local Indian Ocean air–sea processes, which can be triggered by anomalous easterly winds over the eastern equatorial Indian Ocean (e.g., Hong et al. 2008; Sun et al. 2015). Thus, without the counteracting effects of El Niño, these independent positive IOD events result in positive ISMR anomalies as described above and can contribute to the variability of PC1 and PC3 of ISMR. Since ENSO and IOD events do not co-occur in the No P↔I experiment (see Fig. S4), the opposite impacts on ISMR (as shown by the regression patterns in Figs. 9e,f) act to enhance the variability of ISMR leading to the increased standard deviations of PC1 and PC3 in this experiment (Figs. 7a,c).

To further understand the damping effect of the direct forcing from Indian Ocean SSTA and the Indo-Pacific interaction on the ISMR–ENSO relationship (as shown in Figs. 9c,e by the larger ENSO–ISMR regression coefficients for these experiments), we examined ENSO's amplitude, determined by the standard deviation of the Niño-3.4 index, and period for each of the CS-LIM experiments (figure not shown). Our results showed that the amplitude of ENSO increases for all seasons in the No I→M and No P↔I experiments relative to that of the CS-LIM control run, and the average length of El Niño events in the No P↔I experiment is significantly longer than that of the control run or observations (i.e., about 19 months in No P↔I compared to about 8–10 months in control run and observation). These results indicate that the direct forcing from the Indian Ocean and Indo-Pacific interaction tend to reduce the amplitude and duration of ENSO events and thus weaken ENSO's impact on ISMR.

The particular mechanisms regarding how the tropical Indo-Pacific interaction acts to reduce the amplitude and duration of ENSO events are not well understood. However, the negative feedback of El Niño–induced basinwide warm SSTA in the tropical Indian Ocean (i.e., positive IOB) on El Niño has been suggested by some previous studies (e.g., Kug and Kang 2006; Dayan et al. 2015). The warm SSTA of the IOB, which reaches its maximum amplitude a few months after the El Niño peak, induces easterly wind anomalies in the western tropical Pacific which may trigger a quicker transition to La Niña by causing oceanic upwelling Kelvin waves (Kug and Kang 2006). Since this negative feedback between ENSO in the tropical Pacific and the ENSO-induced IOB mode in the tropical Indian Ocean is effectively removed in the No P↔I experiment, it may contribute to the larger amplitude and duration of ENSO events as well as the stronger ENSO–ISMR relationship in the No P↔I experiment. Alternatively, the increased amplitude of ENSO in the No I→M experiment suggests a potential negative feedback mechanism on ENSO through the Indian Ocean's impacts on the monsoon. A thorough investigation of the role of Indian Ocean SSTAs and the Indo-Pacific interaction in damping ISMR variability and the relevant mechanisms is beyond the scope of our current study but is an interesting topic for our future research.

4. Summary and discussion

To isolate the impacts of tropical Indo-Pacific SSTAs on Asian monsoon precipitation variability, especially on Indian summer monsoon rainfall, we applied a cyclostationary linear inverse model (CS-LIM). Two observational datasets of monthly SST and monthly GPCC precipitation were analyzed over the 1950–2019 70-yr period and used to construct the CS-LIM. In addition to the CS-LIM control run, representing the complete solution and used to validate the model against observations, a series of process experiments were performed. These experiments were designed to isolate the individual impacts on the interannual variability of monsoon precipitation due to the direct forcing from Pacific SSTA, the direct forcing from Indian Ocean SSTA, and the interaction between them (Table 1). For all experiments, the CS-LIM was integrated forward in time for 70 000 years (1000 times the 70-yr observational period). Results of the model integrations demonstrate that the CS-LIM control run is capable of reproducing much of the observed patterns of precipitation variability, including its seasonality, over the broad Asian monsoon region (Fig. 1). This allowed us to conclude that it is an effective tool for this study.

Using the results from the CS-LIM process experiments, we obtained the following principal conclusions regarding the impacts of isolated tropical Pacific and Indian Ocean SSTAs on precipitation variability over the Asian monsoon region:

1) The direct forcing from the Pacific enhances Asian monsoon precipitation variability over certain regions and seasons, which can be largely attributed to ENSO's impact on the monsoon during the different stages of ENSO's development (Figs. 2a–d).
2) Many of those same regions impacted by ENSO exhibit a reduction in precipitation variability due to the direct forcing from Indian Ocean SSTAs, which is further reinforced by the Indo-Pacific interaction (Figs. 2e–l). This effect occurs especially over India during the ISMR season of JJA.

The enhanced ISMR variability due to the direct forcing from the Pacific and reduced ISMR variability due to the direct forcing from Indian Ocean SSTAs agree with the results from previous studies. However, the strong damping effect on ISMR due to the Indo-Pacific interaction is a new result and was investigated further to consider the tropical Pacific and Indian Ocean SSTAs impacts on the leading three EOF modes of ISMR.

We first demonstrated that the CS-LIM control run can successfully reproduce the observed EOF patterns of ISMR (Fig. 3) as well as their observed relationships with tropical Pacific and Indian Ocean SSTAs (Figs. 4–6). Consistent with previous studies, we find that the first EOF mode, which is associated with precipitation anomalies of the same sign over most of the Indian subcontinent, is related to developing ENSO events in the tropical Pacific. The second EOF mode of ISMR exhibits a wet northeast–dry southwest dipole pattern of precipitation

anomalies over India. It is negatively correlated with the previous year's ENSO events and the closely related IOB mode in observations, as shown by previous studies, and in the CS-LIM control run. The third EOF mode of ISMR, which is associated with reduced precipitation over southern and northeastern India and increased precipitation over the central Indian monsoon region, is positively correlated with developing ENSO and IOD events in both observations and the CS-LIM control run, consistent with previous studies.

Our results from the India-only CS-LIM process experiments reveal the following conclusions about the impacts of isolated tropical Pacific and Indian Ocean SSTAs on ISMR:

1) The enhanced variability of ISMR due to the direct forcing from Pacific SSTA can be largely explained by ENSO's direct impacts on the first and third EOFs of ISMR. This is supported by the reduced standard deviations of ISMR PC1 and PC3 when we remove the direct forcing from the Pacific onto the monsoon (Figs. 7a,c) and agrees with the strongly reduced ENSO–PC1 (Fig. 8b) and ENSO–PC3 (Fig. S2) correlations in the No P→M experiment. However, the relatively weak decrease in the standard deviations of these PCs, especially for PC1, suggests that without the direct forcing from ENSO on ISMR, tropical Indian Ocean SSTA and other forcings still generate variability of ISMR PC1 (and PC3). For example, positive IOD events that do not co-occur with El Niño events can induce a negative EOF1 pattern of ISMR (as demonstrated by the IOD regression pattern of ISMR in the No P↔I experiment; Fig. 9f).
2) The reduced variability of ISMR due to the direct forcing from Indian Ocean SSTA is the result of Indian Ocean SSTA's acting to oppose ENSO's impacts on the first and third EOFs of ISMR, which is consistent with previous studies. When we remove the direct forcing from the Indian Ocean onto the monsoon, the PC1–ENSO correlation increases (Fig. 8c), and the ENSO regression pattern, which shows a combined EOF1 and EOF3 pattern, gets stronger (Fig. 9b). This agrees with the increase in the standard deviations of PC1 and PC3 in the No I→M experiment (Figs. 7a,c) and can also be explained by the opposing impacts from ENSO and ENSO-induced IOD events, which is effectively removed in this experiment (Figs. 9b,e).
3) The new results from our study specifically reveal the importance of the tropical Indo-Pacific SSTA interaction in damping the variability of ISMR. Similar to the results for the No I→M experiment, the increased standard deviations of PC1 and PC3 can be explained by the Indo-Pacific interaction opposing ENSO's direct impacts on ISMR. This is supported by the increased ENSO–PC1 and ENSO–PC3 correlations and ENSO's stronger impacts on ISMR in the No P↔I experiment (Figs. 8d and 9c). Additionally, we find that ENSO and IOD events do not co-occur when we remove the tropical Indo-Pacific interaction, as shown by the ENSO–IOD correlation being close to zero (Fig. S4). Thus, the opposite impacts from developing ENSO and IOD events (Figs. 9c,f), which occur independently, can increase the variability of PC1 and PC3 in this experiment. Our results also suggest that tropical Indo-Pacific interaction acts to reduce the magnitude of ENSO and shorten its period, which may also contribute to the damping of ISMR variability; however, these results require further investigation.

While we have demonstrated the ability of the CS-LIM to capture many of the observed relationships between tropical Indo-Pacific SSTAs and Asian monsoon precipitation, there are some limitations in the CS-LIM method. First, the relatively short observation record used to construct the linear dynamical operators for each season of the CS-LIM may not be long enough to accurately capture the full linear dynamics of the system for investigation of the interannual variability. This is because the CS-LIM assumes that the dynamics captured by the linear operators are stationary and thus do not evolve in time. This may not always be a valid assumption, as positive and negative phases of multidecadal and longer time-scale climate variability modes, such as the interdecadal Pacific oscillation (IPO) and Atlantic multidecadal variability (AMV), can modulate the ENSO–IOD–monsoon relationships. Indeed, previous studies have identified a shift in the interactions between the tropical Pacific and Indian Ocean, as well as with the Asian monsoon, around the 1970–80s (e.g., Cherchi and Navarra 2013; Chakravorty et al. 2016; Hrudya et al. 2021b). Our 70-yr observational period from 1950 to 2019, however, spans both the positive and negative phases of the IPO and AMO (not shown) and thus may be able to construct reasonably stationary dynamics of the linear operators, which can be affected by multidecadal and longer time-scale climate modes. The increasing atmospheric greenhouse gas concentrations and natural external forcings of the climate system may also affect the stationarity of the linear operators in the CS-LIM. While insight into the limitation of the short time record could be addressed by performing similar CS-LIM analysis on model simulations with longer records, such as those from CMIP6 models with controlled external forcings, one would have to take into account the added uncertainty due to model biases.

Despite the limitations, this study reveals the distinct impacts of isolated (i.e., direct forcing from) tropical Pacific and Indian Ocean SSTAs on Asian monsoon precipitation variability and offers new insight into how the Indo-Pacific interaction damps the ISMR variability. These findings may have important applications for monsoon prediction and predictability. Further CS-LIM analysis could include exploring the spatial structure of the noise covariance matrix or eigen analysis of the linear dynamical operators. Additionally, the roles played by the SSTA in the Atlantic Ocean and its interaction with the Indo-Pacific SSTAs, as well as the decadal and multidecadal variability of these relationships, deserve a thorough investigation. Successful simulations of the relationships between the monsoon, ENSO, and IOD, as well as other modes of climate variability in the state-of-the-art climate models, are essential for an improved monsoon prediction, which will benefit our human society. Consequently, investigating how well these tropical SSTA–monsoon

relationships are represented in CMIP6 models and examining how they may change under a warming climate over the next few decades and century are important areas of our future research. Retrospective forecasts constructed from the LIM (e.g., following Kido et al. 2023) could also provide useful information about the prediction skill of monsoon precipitation associated with the Indo-Pacific SSTA forcings.

Acknowledgments. E. G., W. H., and L. Z. are supported by the National Science Foundation Award NSF-AGS 1935279. Part of the work was completed while WH was visiting the International Space Science Institute (ISSI), Bern, Switzerland, in the summer of 2023. She thanks the Johannes Geiss Fellowship from ISSI for providing travel support. L. Z. is supported by the development fund of the South China Sea Institute of Oceanology of the Chinese Academy of Sciences SCSIO202203. E. D. L. and E. G. would like to recognize support from DOE Award DE-SC0023228.

Data availability statement. The HadISST and ERSST.v5 observational SST datasets are available at http://psl.noaa.gov/data/gridded/data.noaa.ersst.v5.html and http://www.metoffice.gov.uk/hadobs/hadisst/data/download.html, respectively. The GPCC land precipitation dataset is available at http://psl.noaa.gov/data/gridded/data.gpcc.html.

REFERENCES

Aiming, W., and N. Yunqi, 1997: The influence of Tibetan Plateau on the interannual variability of Asian monsoon. *Adv. Atmos. Sci.*, **14**, 491–504, https://doi.org/10.1007/s00376-997-0067-0.

Annamalai, H., and P. Liu, 2005: Response of the Asian summer monsoon to changes in El Niño properties. *Quart. J. Roy. Meteor. Soc.*, **131**, 805–831, https://doi.org/10.1256/qj.04.08.

——, ——, and S.-P. Xie, 2005: Southwest Indian Ocean SST variability: Its local effect and remote influence on Asian monsoons. *J. Climate*, **18**, 4150–4167, https://doi.org/10.1175/JCLI3533.1.

Ashok, K., Z. Guan, and T. Yamagata, 2001: Impact of the Indian Ocean dipole on the relationship between the Indian monsoon rainfall and ENSO. *Geophys. Res. Lett.*, **28**, 4499–4502, https://doi.org/10.1029/2001GL013294.

——, ——, N. H. Saji, and T. Yamagata, 2004: Individual and combined influences of ENSO and the Indian Ocean dipole on the Indian summer monsoon. *J. Climate*, **17**, 3141–3155, https://doi.org/10.1175/1520-0442(2004)017<3141:IACIOE>2.0.CO;2.

——, S. K. Behera, S. A. Rao, H. Weng, and T. Yamagata, 2007: El Niño Modoki and its possible teleconnection. *J. Geophys. Res.*, **112**, C11007, https://doi.org/10.1029/2006JC003798.

Capotondi, A., and Coauthors, 2015: Understanding ENSO diversity. *Bull. Amer. Meteor. Soc.*, **96**, 921–938, https://doi.org/10.1175/BAMS-D-13-00117.1.

Chakravorty, S., C. Gnanaseelan, and P. A. Pillai, 2016: Combined influence of remote and local SST forcing on Indian Summer Monsoon Rainfall variability. *Climate Dyn.*, **47**, 2817–2831, https://doi.org/10.1007/s00382-016-2999-5.

Chen, Z., Z. Wen, R. Wu, and Y. Du, 2017: Roles of tropical SST anomalies in modulating the western north Pacific anomalous cyclone during strong La Niña decaying years. *Climate Dyn.*, **49**, 633–647, https://doi.org/10.1007/s00382-016-3364-4.

Cherchi, A., and A. Navarra, 2013: Influence of ENSO and of the Indian Ocean Dipole on the Indian summer monsoon variability. *Climate Dyn.*, **41**, 81–103, https://doi.org/10.1007/s00382-012-1602-y.

Chowdary, J. S., A. B. Bandgar, C. Gnanaseelan, and J.-J. Luo, 2015: Role of tropical Indian Ocean air–sea interactions in modulating Indian summer monsoon in a coupled model. *Atmos. Sci. Lett.*, **16**, 170–176, https://doi.org/10.1002/asl2.561.

——, D. Patekar, G. Srinivas, C. Gnanaseelan, and A. Parekh, 2019: Impact of the Indo-Western Pacific Ocean capacitor mode on South Asian summer monsoon rainfall. *Climate Dyn.*, **53**, 2327–2338, https://doi.org/10.1007/s00382-019-04850-w.

Clark, C. O., J. E. Cole, and P. J. Webster, 2000: Indian Ocean SST and Indian summer rainfall: Predictive relationships and their decadal variability. *J. Climate*, **13**, 2503–2519, https://doi.org/10.1175/1520-0442(2000)013<2503:IOSAIS>2.0.CO;2.

Dandi, R. A., J. S. Chowdary, P. A. Pillai, N. S. S. Sidhan, K. Koteswararao, and S. S. V. S. Ramakrishna, 2020: Impact of El Niño Modoki on Indian summer monsoon rainfall: Role of western north Pacific circulation in observations and CMIP5 models. *Int. J. Climatol.*, **40**, 2117–2133, https://doi.org/10.1002/joc.6322.

Dayan, H., T. Izumo, J. Vialard, M. Lengaigne, and S. Masson, 2015: Do regions outside the tropical Pacific influence ENSO through atmospheric teleconnections? *Climate Dyn.*, **45**, 583–601, https://doi.org/10.1007/s00382-014-2254-x.

Fan, F., R. Lin, X. Fang, F. Xue, F. Zheng, and J. Zhu, 2021: Influence of the eastern Pacific and central Pacific types of ENSO on the South Asian summer monsoon. *Adv. Atmos. Sci.*, **38**, 12–28, https://doi.org/10.1007/s00376-020-0055-1.

Fan, L., S.-I. Shin, Q. Liu, and Z. Liu, 2013: Relative importance of tropical SST anomalies in forcing East Asian summer monsoon circulation. *Geophys. Res. Lett.*, **40**, 2471–2477, https://doi.org/10.1002/grl.50494.

Fischer, A. S., P. Terray, E. Guilyardi, S. Gualdi, and P. Delecluse, 2005: Two independent triggers for the Indian Ocean dipole/zonal mode in a coupled GCM. *J. Climate*, **18**, 3428–3449, https://doi.org/10.1175/JCLI3478.1.

Fu, C., 2003: Potential impacts of human-induced land cover change on East Asia monsoon. *Global Planet. Change*, **37**, 219–229, https://doi.org/10.1016/S0921-8181(02)00207-2.

Ganguly, D., P. J. Rasch, H. Wang, and J.-H. Yoon, 2012: Climate response of the South Asian monsoon system to anthropogenic aerosols. *J. Geophys. Res.*, **117**, D13209, https://doi.org/10.1029/2012JD017508.

Gao, C., and G. Li, 2023: Asymmetric effect of ENSO on the maritime continent precipitation in decaying summers. *Climate Dyn.*, **61**, 2839–2852, https://doi.org/10.1007/s00382-023-06716-8.

Ge, F., S. Zhu, F. Sielmann, K. Fraedrich, X. Zhu, L. Zhang, X. Zhi, and H. Wang, 2021: Precipitation over Indochina during the monsoon transition: Modulation by Indian Ocean and ENSO regimes. *Climate Dyn.*, **57**, 2491–2504, https://doi.org/10.1007/s00382-021-05817-6.

Hong, C.-C., M.-M. Lu, and M. Kanamitsu, 2008: Temporal and spatial characteristics of positive and negative Indian Ocean dipole with and without ENSO. *J. Geophys. Res.*, **113**, D08107, https://doi.org/10.1029/2007JD009151.

Hrudya, P. H., H. Varikoden, and R. Vishnu, 2021a: A review on the Indian summer monsoon rainfall, variability and its

association with ENSO and IOD. *Meteor. Atmos. Phys.*, **133** (1), 1–14, https://doi.org/10.1007/s00703-020-00734-5.

——, ——, and ——, 2021b: Changes in the relationship between Indian Ocean dipole and Indian summer monsoon rainfall in early and recent multidecadal epochs during different phases of monsoon. *Int. J. Climatol.*, **41**, E305–E318, https://doi.org/10.1002/joc.6685.

Huang, B., and Coauthors, 2017: Extended Reconstructed Sea Surface Temperature, version 5 (ERSSTv5): Upgrades, validations, and intercomparisons. *J. Climate*, **30**, 8179–8205, https://doi.org/10.1175/JCLI-D-16-0836.1.

Izumo, T., C. B. Montégut, J.-J. Luo, S. K. Behera, S. Masson, and T. Yamagata, 2008: The role of the western Arabian Sea upwelling in Indian monsoon rainfall variability. *J. Climate*, **21**, 5603–5623, https://doi.org/10.1175/2008JCLI2158.1.

——, and Coauthors, 2010: Influence of the state of the Indian Ocean Dipole on the following year's El Niño. *Nat. Geosci.*, **3**, 168–172, https://doi.org/10.1038/ngeo760.

Ju, J., and J. Slingo, 1995: The Asian summer monsoon and ENSO. *Quart. J. Roy. Meteor. Soc.*, **121**, 1133–1168, https://doi.org/10.1002/qj.49712152509.

Kido, S., I. Richter, T. Tozuka, and P. Chang, 2023: Understanding the interplay between ENSO and related tropical SST variability using linear inverse models. *Climate Dyn.*, **61**, 1029–1048, https://doi.org/10.1007/s00382-022-06484-x.

Klein, S. A., B. J. Soden, and N.-C. Lau, 1999: Remote sea surface temperature variations during ENSO: Evidence for a tropical atmospheric bridge. *J. Climate*, **12**, 917–932, https://doi.org/10.1175/1520-0442(1999)012<0917:RSSTVD>2.0.CO;2.

Kug, J.-S., and I.-S. Kang, 2006: Interactive feedback between ENSO and the Indian Ocean. *J. Climate*, **19**, 1784–1801, https://doi.org/10.1175/JCLI3660.1.

Lau, N.-C., and M. J. Nath, 2000: Impact of ENSO on the variability of the Asian–Australian monsoons as simulated in GCM experiments. *J. Climate*, **13**, 4287–4309, https://doi.org/10.1175/1520-0442(2000)013<4287:IOEOTV>2.0.CO;2.

Li, C., and M. Yanai, 1996: The onset and interannual variability of the Asian summer monsoon in relation to land–sea thermal contrast. *J. Climate*, **9**, 358–375, https://doi.org/10.1175/1520-0442(1996)009<0358:TOAIVO>2.0.CO;2.

Li, G., C. Gao, B. Lu, and H. Chen, 2021: Inter-annual variability of spring precipitation over the Indo-China Peninsula and its asymmetric relationship with El Niño-Southern Oscillation. *Climate Dyn.*, **56**, 2651–2665, https://doi.org/10.1007/s00382-020-05609-4.

Li, H., A. Dai, T. Zhou, and J. Lu, 2010: Responses of East Asian summer monsoon to historical SST and atmospheric forcing during 1950–2000. *Climate Dyn.*, **34**, 501–514, https://doi.org/10.1007/s00382-008-0482-7.

Li, Z., and Coauthors, 2016: Aerosol and monsoon climate interactions over Asia. *Rev. Geophys.*, **54**, 866–929, https://doi.org/10.1002/2015RG000500.

Liu, X., and M. Yanai, 2002: Influence of Eurasian spring snow cover on Asian summer rainfall. *Int. J. Climatol.*, **22**, 1075–1089, https://doi.org/10.1002/joc.784.

——, and B. Dong, 2013: Influence of the Tibetan Plateau uplift on the Asian monsoon-arid environment evolution. *Chin. Sci. Bull.*, **58**, 4277–4291, https://doi.org/10.1007/s11434-013-5987-8.

Loschnigg, J., G. A. Meehl, P. J. Webster, J. M. Arblaster, and G. P. Compo, 2003: The Asian monsoon, the tropospheric biennial oscillation, and the Indian Ocean zonal mode in the NCAR CSM. *J. Climate*, **16**, 1617–1642, https://doi.org/10.1175/1520-0442(2003)016<1617:TAMTTB>2.0.CO;2.

Meehl, G. A., 1997: The south Asian monsoon and the tropospheric biennial oscillation. *J. Climate*, **10**, 1921–1943, https://doi.org/10.1175/1520-0442(1997)010<1921:TSAMAT>2.0.CO;2.

——, J. M. Arblaster, and J. Loschnigg, 2003: Coupled ocean–atmosphere dynamical processes in the tropical Indian and Pacific Oceans and the TBO. *J. Climate*, **16**, 2138–2158, https://doi.org/10.1175/2767.1.

Mishra, V., B. V. Smoliak, D. P. Lettenmaier, and J. M. Wallace, 2012: A prominent pattern of year-to-year variability in Indian summer monsoon rainfall. *Proc. Natl. Acad. Sci. USA*, **109**, 7213–7217, https://doi.org/10.1073/pnas.1119150109.

Mohino, E., B. Rodríguez-Fonseca, C. R. Mechoso, S. Gervois, P. Ruti, and F. Chauvin, 2011: Impacts of the tropical Pacific/Indian Oceans on the seasonal cycle of the West African monsoon. *J. Climate*, **24**, 3878–3891, https://doi.org/10.1175/2011JCLI3988.1.

Newman, M., 2007: Interannual to decadal predictability of tropical and North Pacific sea surface temperatures. *J. Climate*, **20**, 2333–2356, https://doi.org/10.1175/JCLI4165.1.

——, M. A. Alexander, and J. D. Scott, 2011: An empirical model of tropical ocean dynamics. *Climate Dyn.*, **37**, 1823–1841, https://doi.org/10.1007/s00382-011-1034-0.

North, G. R., T. L. Bell, R. F. Cahalan, and F. J. Moeng, 1982: Sampling errors in the estimation of empirical orthogonal functions. *Mon. Wea. Rev.*, **110**, 699–706, https://doi.org/10.1175/1520-0493(1982)110<0699:SEITEO>2.0.CO;2.

Penland, C., and L. Matrosova, 1994: A balance condition for stochastic numerical models with application to the El Niño-Southern Oscillation. *J. Climate*, **7**, 1352–1372, https://doi.org/10.1175/1520-0442(1994)007<1352:ABCFSN>2.0.CO;2.

——, and P. D. Sardeshmukh, 1995: The optimal growth of tropical sea surface temperature anomalies. *J. Climate*, **8**, 1999–2024, https://doi.org/10.1175/1520-0442(1995)008<1999:TOGOTS>2.0.CO;2.

Rayner, N. A., D. E. Parker, E. B. Horton, C. K. Folland, L. V. Alexander, D. P. Rowell, E. C. Kent, and K. A. Kaplan, 2003: Global analyses of sea surface temperature, sea ice, and night marine air temperature since the late nineteenth century. *J. Geophys. Res.*, **108**, 4407, https://doi.org/10.1029/2002JD002670.

Rong, X., R. Zhang, and T. Li, 2010: Impacts of Atlantic sea surface temperature anomalies on Indo-East Asian summer monsoon-ENSO relationship. *Chin. Sci. Bull.*, **55**, 2458–2468, https://doi.org/10.1007/s11434-010-3098-3.

Saji, N. H., B. N. Goswami, P. N. Vinayachandran, and T. Yamagata, 1999: A dipole mode in the tropical Indian Ocean. *Nature*, **401**, 360–363, https://doi.org/10.1038/43854.

Sankar-Rao, M., K. M. Lau, and S. Yang, 1996: On the relationship between Eurasian snow cover and the Asian summer monsoon. *Int. J. Climatol.*, **16**, 605–616, https://doi.org/10.1002/(SICI)1097-0088(199606)16:6<605::AID-JOC41>3.0.CO;2-P.

Schneider, U., A. Becker, P. Finger, E. Rustemeier, and M. Ziese, 2020: GPCC full data monthly version 2020 at 2.5°: Monthly land-surface precipitation from rain-gauges built on GTS-based and historic data. Global Precipitation Climatology Centre (GPCC) at Deutscher Wetterdienst, accessed 25 July 2023, https://doi.org/10.5676/DWD_GPCC/FD_M_V2020_250.

Schott, F. A., S.-P. Xie, and J. P. McCreary Jr., 2009: Indian Ocean circulation and climate variability. *Rev. Geophys.*, **47**, RG1002, https://doi.org/10.1029/2007RG000245.

Shin, S.-I., P. D. Sardeshmukh, M. Newman, C. Penland, and M. A. Alexander, 2021: Impact of annual cycle on ENSO variability and predictability. *J. Climate*, **34**, 171–193, https://doi.org/10.1175/JCLI-D-20-0291.1.

Shukla, R. P., and B. Huang, 2016: Interannual variability of the Indian summer monsoon associated with the air–sea feedback in the northern Indian Ocean. *Climate Dyn.*, **46**, 1977–1990, https://doi.org/10.1007/s00382-015-2687-x.

Sun, S., J. Lan, Y. Fang, Tana, and X. Gao, 2015: A triggering mechanism for the Indian Ocean dipoles independent of ENSO. *J. Climate*, **28**, 5063–5076, https://doi.org/10.1175/JCLI-D-14-00580.1.

Syed, F. S., and F. Kucharski, 2016: Statistically related coupled modes of South Asian summer monsoon interannual variability in the tropics. *Atmos. Sci. Lett.*, **17**, 183–189, https://doi.org/10.1002/asl.641.

Terray, P., P. Delecluse, S. Labattu, and L. Terray, 2003: Sea surface temperature associations with the late Indian summer monsoon. *Climate Dyn.*, **21**, 593–618, https://doi.org/10.1007/s00382-003-0354-0.

Ummenhofer, C. C., A. Sen Gupta, Y. Li, A. S. Taschetto, and M. H. England, 2011: Multi-decadal modulation of the El Niño–Indian monsoon relationship by Indian Ocean variability. *Environ. Res. Lett.*, **6**, 034006, https://doi.org/10.1088/1748-9326/6/3/034006.

——, R. D. D'Arrigo, K. J. Anchukaitis, B. M. Buckley, and E. R. Cook, 2013: Links between Indo-Pacific climate variability and drought in the Monsoon Asia Drought Atlas. *Climate Dyn.*, **40**, 1319–1334, https://doi.org/10.1007/s00382-012-1458-1.

Vernekar, A. D., J. Zhou, and J. Shukla, 1995: The effect of Eurasian snow cover on the Indian monsoon. *J. Climate*, **8**, 248–266, https://doi.org/10.1175/1520-0442(1995)008<0248:TEOESC>2.0.CO;2.

Vimont, D. J., M. Newman, D. S. Battisti, and S.-I. Shin, 2022: The role of seasonality and the ENSO mode in central and East Pacific ENSO growth and evolution. *J. Climate*, **35**, 3195–3209, https://doi.org/10.1175/JCLI-D-21-0599.1.

Wang, B., R. Wu, and T. Li, 2003: Atmosphere–warm ocean interaction and its impacts on Asian–Australian monsoon variation. *J. Climate*, **16**, 1195–1211, https://doi.org/10.1175/1520-0442(2003)16<1195:AOIAII>2.0.CO;2.

Wang, Z., R. Wu, and Y. Wang, 2022: Impacts of the East Asian winter monsoon on winter precipitation variability over East Asia-western North Pacific. *Climate Dyn.*, **58**, 3041–3055, https://doi.org/10.1007/s00382-021-06086-z.

Webster, P. J., and S. Yang, 1992: Monsoon and ENSO: Selectively interactive systems. *Quart. J. Roy. Meteor. Soc.*, **118**, 877–926, https://doi.org/10.1002/qj.49711850705.

——, V. O. Magaña, T. N. Palmer, J. Shukla, R. A. Tomas, M. Yanai, and T. Yasunari, 1998: Monsoons: Processes, predictability, and the prospects for prediction. *J. Geophys. Res.*, **103**, 14 451–14 510, https://doi.org/10.1029/97JC02719.

——, A. M. Moore, J. P. Loschnigg, and R. R. Leben, 1999: Coupled ocean–atmosphere dynamics in the Indian Ocean during 1997–98. *Nature*, **401**, 356–360, https://doi.org/10.1038/43848.

——, C. Clark, G. Cherikova, J. Fasullo, W. Han, J. Loschnigg, and K. Sahami, 2002: The monsoon as a self-regulating coupled ocean—atmosphere system. *Int. Geophys.*, **83**, 198–219, https://doi.org/10.1016/S0074-6142(02)80168-1.

Wu, B., T. Li, and T. Zhou, 2010: Relative contributions of the Indian Ocean and local SST anomalies to the maintenance of the western North Pacific anomalous anticyclone during the El Niño decaying summer. *J. Climate*, **23**, 2974–2986, https://doi.org/10.1175/2010JCLI3300.1.

Wu, X., G. Li, W. Jiang, S.-M. Long, and B. Lu, 2021: Asymmetric relationship between ENSO and the tropical Indian Ocean summer SST anomalies. *J. Climate*, **34**, 5955–5969, https://doi.org/10.1175/JCLI-D-20-0546.1.

Xie, S.-P., K. Hu, J. Hafner, H. Tokinaga, Y. Du, G. Huang, and T. Sampe, 2009: Indian Ocean capacitor effect on Indo–Western Pacific climate during the summer following El Niño. *J. Climate*, **22**, 730–747, https://doi.org/10.1175/2008JCLI2544.1.

——, Y. Kosaka, Y. Du, K. Hu, J. S. Chowdary, and G. Huang, 2016: Indo-western Pacific ocean capacitor and coherent climate anomalies in post-ENSO summer: A review. *Adv. Atmos. Sci.*, **33**, 411–432, https://doi.org/10.1007/s00376-015-5192-6.

Yang, J., Q. Liu, S.-P. Xie, Z. Liu, and L. Wu, 2007: Impact of the Indian Ocean SST basin mode on the Asian summer monsoon. *Geophys. Res. Lett.*, **34**, L02708, https://doi.org/10.1029/2006GL028571.

——, ——, and Z. Liu, 2010: Linking observations of the Asian monsoon to the Indian Ocean SST: Possible roles of Indian Ocean Basin mode and dipole mode. *J. Climate*, **23**, 5889–5902, https://doi.org/10.1175/2010JCLI2962.1.

Yang, Y., R. Wu, and C. Wang, 2020: Individual and combined impacts of tropical Indo-Pacific SST anomalies on interannual variation of the Indochina peninsular precipitation. *J. Climate*, **33**, 1069–1088, https://doi.org/10.1175/JCLI-D-19-0262.1.

Yu, J.-Y., 2008: Understanding the El Niño–Southern Oscillation and its interactions with the Indian Ocean and monsoon. *Recent Progress in Atmospheric Sciences: Applications to the Asia-Pacific Region*, World Scientific Publishing Company, 3–22.

——, C. R. Mechoso, J. C. McWilliams, and A. Arakawa, 2002: Impacts of the Indian Ocean on the ENSO cycle. *Geophys. Res. Lett.*, **29**, 1208, https://doi.org/10.1029/2001GL014098.

Yuan, Y., H. Yang, W. Zhou, and C. Li, 2008: Influences of the Indian Ocean dipole on the Asian summer monsoon in the following year. *Int. J. Climatol.*, **28**, 1849–1859, https://doi.org/10.1002/joc.1678.

Zhang, L., W. Han, G. A. Meehl, A. Hu, N. Rosenbloom, T. Shinoda, and M. J. McPhaden, 2021a: Diverse impacts of the Indian Ocean dipole on El Niño–Southern Oscillation. *J. Climate*, **34**, 9057–9070, https://doi.org/10.1175/JCLI-D-21-0085.1.

——, G. Wang, M. Newman, and W. Han, 2021b: Interannual to decadal variability of tropical Indian Ocean sea surface temperature: Pacific influence versus local internal variability. *J. Climate*, **34**, 2669–2684, https://doi.org/10.1175/JCLI-D-20-0807.1.

Zhang, Y., S.-P. Xie, Y. Kosaka, and J.-C. Yang, 2018: Pacific decadal oscillation: Tropical Pacific forcing versus internal variability. *J. Climate*, **31**, 8265–8279, https://doi.org/10.1175/JCLI-D-18-0164.1.

——, W. Zhou, X. Wang, X. Wang, R. Zhang, Y. Li, and J. Gan, 2022: IOD, ENSO, and seasonal precipitation variation over Eastern China. *Atmos. Res.*, **270**, 106042, https://doi.org/10.1016/j.atmosres.2022.106042.

Zhao, Y., M. Newman, A. Capotondi, E. D. Lorenzo, and D. Sun, 2021: Removing the effects of tropical dynamics from North Pacific climate variability. *J. Climate*, **34**, 9249–9265, https://doi.org/10.1175/JCLI-D-21-0344.1.

——, E. Di Lorenzo, M. Newman, A. Capotondi, and S. Stevenson, 2023: A Pacific tropical decadal variability challenge for climate models. *Geophys. Res. Lett.*, **50**, e2023GL104037, https://doi.org/10.1029/2023GL104037.